Aus der Klinik für Strahlentherapie und Radioonkologie
der Medizinischen Fakultät Mannheim, Universität Heidelberg
(Kommissarischer Direktor: Dr. med. Michael Ehmann)

Treatment plan optimization based on biologically effective dose in Gamma Knife radiotherapy

Inauguraldissertation
zur Erlangung des Doctor scientiarum humanarum (Dr. sc. hum.)
der
Medizinischen Fakultät Mannheim
der Ruprecht-Karls-Universität
zu
Heidelberg

vorgelegt von
Juliana Binti Mohd Radzi

aus
Kelantan, Malaysia
2020

Dekan: Herr Prof. Dr. med. Sergij Goerdt
Referent: Herr Prof. Dr. med. Frederik Wenz

TABLE OF CONTENTS

LIST OF FIGURES

LIST OF TABLES

LIST OF ABBREVIATIONS

3D	Three-Dimensional
BED	Biological Effective Dose
BOT	Beam-on Time
CBCT	Cone Beam Computed Tomography
CERR	Computational Environment for Radiological Research
CT	Computed Tomography
Co	Cobalt
DICOM	Digital Imaging and Communications in Medicine
DNA	Deoxyribonucleic Acid
GBM	Glioblastoma
GK	Gamma Knife
GKRS	Gamma Knife Radiosurgery
HU	Hounsfield Unit
IR	Infrared
IFMM	Intra-fraction Motion Management
LGP	Leksell Gamma Plan
LINAC	Linear Accelerator
LQ	Linear Quadratic
MRI	Magnetic Resonance Imaging
OAR	Organ at Risk
oBED	overall Biological Effective Dose
PTV	Planning Treatment Volume
ROI	Region of Interest
SF	Survival Fraction
SRS	Stereotactic Radiosurgery
TMR	Tissue Maximum Ratio
TN	Trigeminal Neuralgia
TPS	Treatment Planning System
VS	Vestibular Schwannoma
WBRT	Whole Brain Radiation Therapy

1 INTRODUCTION

1.1 Motivation

Intracranial stereotactic radiosurgery (SRS) is generally used to treat malignant and benign brain lesions and represents a non-surgical alternative to complex brain surgery. This technique precisely delivers high doses of highly focused ionizing radiation to a target region, which allows an increased therapeutic effect in the lesions with a low damage to the surrounding healthy tissues [1]. The devices most commonly used for SRS are the Gamma Knife (GK) (Elekta AB, Stockholm, Sweden) and linear accelerators (LINACs). However, other systems such as CyberKnife (Accuray, Sunnyvale, CA, USA), TomoTherapy (Accuray, Sunnyvale, CA, USA) and proton therapy are also employed for this kind of treatment. Each of these systems and modalities has particular advantages and drawbacks [2]. Typically, a computed tomography (CT) scan and a magnetic resonance imaging (MRI) scan are used together in SRS treatment planning to precisely deliver an individualized treatment to the patients. The MRI scan is used for tumor definition due to its high soft-tissue contrast while the CT scan is used for attenuation correction because of the correlation between Hounsfield units (HUs) and the attenuation coefficients.

GK radiosurgery allows to deliver either a single or a few conformal irradiation fractions to the tumor through the intact skull to kill or sterilize clonogenic tumor cells. GK has been utilized to treat malignant and benign brain tumors, arteriovenous malformations (AVMs) and functional disorders [3]. Leksell Gamma Knife® Icon™ is the newest model of Gamma Knife manufactured by Elekta AB, Sweden. The GK Icon integrated with cone-beam CT (CBCT) and other automated features allows single and fractionated treatment with greater accuracy compared to the former models [4,5]. Besides, patient comfort was also improved as treatment with and without the stereotactic frame became possible, and the treatment time is reduced compared to former models. The steep dose gradient outside the target is a unique feature of GK radiosurgery which allows to minimize the radiation dose to the healthy tissues through the combination of immobilization and accurate target localization during the treatment planning process [6].

In treatment with GK, multiple radiation beams, called "shots", are sequentially delivered to produce the prescribed radiation dose in the target region. Each shot is produced using 192 ^{60}Co sources arranged in eight independent and movable sectors with three different collimator sizes each: 4 mm, 8 mm and 16 mm. The sectors can also be blocked or sheered. The dose to the target volume is thus delivered using a combination of shots with different exposure times, isocenters and collimations. The shots will overlap with each other creating a higher dose at the center of the tumor and a steeper dose gradient outside the edge of the tumor volume [7]. Thus, the total dose delivered to the target is determined by the sum of the doses produced by all the shots defined in the treatment plan. The required number of shots depends on the size and

shape of the target. Thus, larger and irregularly shaped targets typically require more shots to create an isodose line according to the target contour [8]. The isodose line produced by a single shot is usually not enough to cover all parts of large target volumes or of targets with irregular shapes [9]. For example, in vestibular schwannoma (a benign primary intracranial tumor), the target volume is usually small, but due to the shape irregularities, more shots are needed to ensure that the isodose line conforms precisely to the target. A smooth and conformal isodose line is essential to ensure an accurate dose delivery to the target, thus sparing the surrounding healthy tissues.

The activity of the GK ^{60}Co sources determine the dose rate and therefore the required exposure time for each shot. Thus, newer sources have higher dose rates which decrease over time according to the ^{60}Co half-life (5.26 years). The treatment efficiency usually decreases with the reduction of dose rates as the total treatment delivery time becomes longer. However, a study on management of the trigeminal nerve showed that the decay of the sources does not affect the treatment outcome (pain relief) even when the source decays approximately to a fourth of the initial dose rate [10]. However, another study found that treatment with a new source (higher dose rates) provides better pain relief and could reduce the pain recurrence rate [11].

Although treatment planning for GK is currently based on physical radiation doses, the consideration of the biological effect both in the target and in the surrounding healthy tissues may produce better outcomes. The biological effect produced by tissue irradiation is usually described by the biologically effective dose (BED). The parameters considered in the calculation of the BED are the dose, the tissue radiosensitivity, the dose rate, the cell repair rate and the irradiation time. The tissue radiosensitivity depends on two effects: lethal DNA damage (produced by a single radiation emission) and sublethal DNA damage (produced by multiple radiation emissions) [12]. The lethal damage does not allow cell repair while DNA repair is possible after sublethal damage. The lethal damage is represented by the α parameter in the linear-quadratic (LQ) model (most commonly accepted model to describe the effect of radiation on cells) while the sublethal damage is represented by the β parameter in the same model [13]. Usually, the tissue radiosensitivity is expressed as the ratio between the α and the β parameters of the LQ model, what is frequently called the α/β ratio.

The sublethal damage repair is the executive action in the tissue after irradiation based on the degree of DNA damage. The sublethal damage repair time depends on the tissue type (early or late responding tissues). Generally, the total completion of the sublethal damage repair takes about 24 h after irradiation. Thus, many incomplete DNA repairs would exist during and after irradiation, especially for long irradiation treatments and when the time interval between treatments is less than 24 h [14]. In addition, the fast components of the repair are essential, especially when the treatment sessions vary between approximately 10 min and 60 min, as in radiosurgery [15]. Therefore, Hopewell et al. suggested that the sublethal damage repair that occurs during a radiosurgery session should be included in the calculation of the BED as the amount of repair influences the total biological effect [15]. Moreover, for GK treatment,

the existence of a time gap between each shot could reduce the effectivity of the absorbed dose to produce a desired biological effect, especially in the target volume, as it allows more sublethal damage repair. This time gap is known as beam-off time, and the dose rate is zero during that time [16]. The beam-off time of the newest GK units is much shorter (6 s) compared to the earlier models (Model B), which is about 6 min [15].

Because of the way the treatment is delivered with the GK, the sequence of shots can influence the biological effect in the regions of interest during a treatment session. Each shot has its own region of action, position in the shot sequence, beam-on time, dose rate and physical dose. Hence, changing the order of the shots will produce a different dose rate pattern in every voxel, which may modify the sublethal damage repair process in the regions of interest. Therefore, for the same shots defined in the treatment plan, the biological response in each voxel of the regions of interest may differ when using different shot sequences. The influence of the intra-fraction dose deposition temporal pattern on the radiobiological response in tissue has been previously reported for radiosurgery with CyberKnife [17]. The probability of sublethal damage repair is higher in voxels with lower dose rates compared to voxels with higher dose rates with similar total doses [18]. Moreover, Andisheh et al. found that the normal tissue BED can be reduced between 2 % to 8 % when changing the shot sequence from the actual clinical sequence for GK [18].

Additionally, some studies have also shown that changes in the dose rate result in variations in the biological response [17,19,20]. Therefore, the dose rates of the GK sources are relevant in the biological effectiveness of the treatment. Thus, newer sources may, in general, produce shots with higher dose rates yielding a higher biological effect.

1.2 Aims

The general purpose of this thesis is to optimize the biological effect during GK treatment by changing the order of the shots resulting from routine treatment planning (which is based on doses only). Improvement in the therapeutic outcome is expected with an optimized sequence as, according to previous studies, [7,18] the biological response varies with the order of the shots. Additionally, BED calculations with three different repair models (mono-exponential, bi-exponential and reciprocal repair) are considered to further investigate the effect of the shot sequence in the GK treatment. Moreover, this study aims at determining the variation in the biological effect produced by the difference between the shot dose rates of a new GK unit and the shot dose rates for a unit whose sources decayed already by one half-life.

2 BACKGROUND

2.1 Leksell Gamma Knife® Icon™

2.1.1 The Leksell Gamma Knife® Icon™ unit

The Leksell Gamma Knife® Icon™ (**Figure 1**) is the latest generation of Gamma Knife manufactured by Elekta (Elekta Instruments, A.B., Stockholm, Sweden) to meet the high demand of intracranial stereotactic radiosurgery. Gamma Knife® Icon™ is an integrated system that provides the possibility for clinicians to carry out single-fraction or fractionated radiotherapy with high precision and accuracy while sparing healthy tissue. In addition, GK treatment can be delivered with or without a stereotactic head frame called G-frame. Thus, treatment of the most complex and critically located targets becomes possible with GK achieving higher conformality than with conventional or sophisticated radiosurgery using LINACs [21]. Furthermore, because of its high precision, no additional safety margin is required around the target volume when using the stereotactic head frame in Gamma Knife radiosurgery (GKRS), which reduces the dose to surrounding tissues.

Figure 1 Leksell Gamma Knife® Icon™ [22].

The inclusion of a cone-beam computed tomography (CBCT) is a new feature of the GK Icon™. The use of a CBCT enables to determine the stereotactic coordinates in the three-dimensional (3D) space without using an invasive frame system [23]. Thus, the stereotactic space coordinates for treatment delivery can be determined by using either the G-frame and a CT scan or CBCT images when the frameless thermoplastic mask is used. For mask treatments, online adaptive planning ensures precision and accuracy in the treatment delivery for every fraction. Moreover, a real-time motion management system with a resolution of 0.15 mm monitors the patient movements in the mask during treatment delivery. The treatment will stop automatically if the patient moves out of a predefined limit.

2.1.2 Gamma Knife® Icon™ sources

Similar to its predecessor, the Leksell Gamma Knife® Perfexion™, the Leksell Gamma Knife® Icon™ uses 192 ^{60}Co sources for treatment delivery. The initial activity of the single source is about 3.0 Ci. Therefore, total initial activity from all sources for a new GK unit exceeds 5000 Ci which, typically produce a dose rate of approximately 300 cGy/min at the isocenter or center of the collimator [24]. ^{60}Co, with a half-life of 5.26 years, decays by emitting two kinds of β⁻ particles followed by two mono-energetic gamma emissions with energies of 1.17 MeV and 1.33 MeV, respectively (**Figure 2**). Only the gamma emissions are used for therapeutic purposes. The effective energy of the Gamma Knife is slightly lower than 1.25 MeV as some photons interact with the ^{60}Co sources themselves and with their encapsulation material, which produces energy loss. In practice, the treatment time for some prescribed doses doubles after approximately five years because of the physical decay of the sources. **Figure 2** shows the decay process of ^{60}Co.
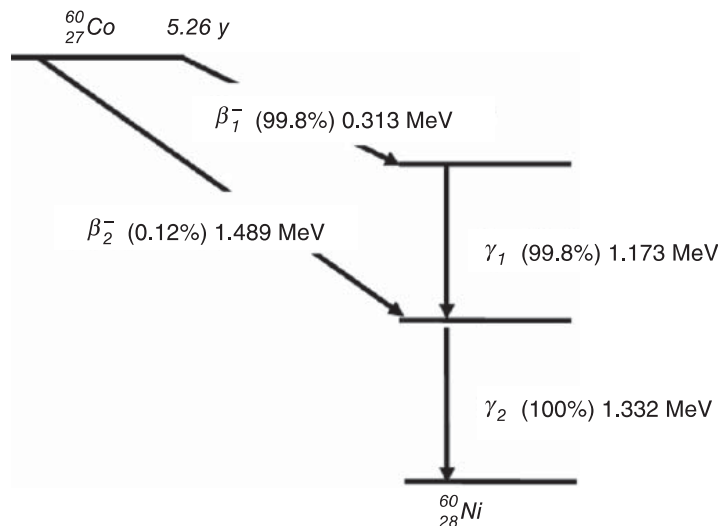
Figure 2 ^{60}Co decay process [25].

The 192 sources of ^{60}Co arranged in a cone-shaped configuration and are distributed in eight movable sectors, each sector consists of 24 sources. There are three available collimator sizes in each sector: 4 mm, 8 mm, and 16 mm. Additionally, each sector can be also blocked. A tungsten block with a thickness of 120 mm is used to determine the collimation in each sector. This tungsten block replaces the multiple helmets for primary and secondary collimators used in previous models. The collimators move independently to achieve the desired sizes for every of the eight sectors, allowing to deliver an isocentric treatment. The size of the collimator determines the diameter of the radiation beams.

The overall dose rate of the GK unit (i.e. the calibration dose rate) is usually determined with all sectors open at the largest collimator size (16 mm). For the GK Icon™, a spherical polystyrene phantom with a radius of 80 mm which allows the insertion of an

ionization chamber in its center is used for the dose rate calibration. The phantom, whose center is located at the radiation isocenter, can be docked in the GK unit. The measured dose rate is used for quality control of the unit when comparing to the machine reference value determined by Monte-Carlo calculations [26]. The calibration dose rate, however, differs from the dose rate in every voxel of the target region as this depends on the number, location, collimation and weighting (i.e. time) of each shot [16]. Therefore, in practice, the concepts of uniform dose distribution or calibration dose rate are irrelevant in GK treatment delivery. Similarly, the total dose per voxel is defined by the location, collimation and weighting of each shot defined in the treatment plan.

2.1.3 Cone-beam Computed Tomography

The cone-beam computed tomography (CBCT) integrated in the Gamma Knife® Icon™ unit consists of a rotating X-ray tube and a 34 cm x 39 cm flat-panel X-ray detector [23]. Both, the X-ray source and the detector, are attached to a supporting arm which allows a 210º rotation during the scanning [23]. The CBCT images determine the stereotactic isocenter for treatment planning and delivery when the thermoplastic mask is used. However, the CBCT isocenters differs from the radiation isocenter of the GK unit. Thus, the co-registration of the CBCT image and the planning diagnostic CT image, which is performed during treatment planning, defines the transformation map between the planned isocenter positions and the stereotactic reference. An additional CBCT image taken just before treatment is used to verify the skull position and therefore guarantees that the dose will be delivered as defined during the treatment planning. Thus, the integrated CBCT enables treatment delivery with high localization accuracy [26].

2.1.4 Intra-fraction Motion Management

The intra-fraction motion management (IFMM) system is another unique feature of the GK Icon™. The IFMM is used to monitor the patient movements during treatment delivery in which the thermoplastic mask is used. According to some studies, the use of a thermoplastic mask, without additional positioning systems, allows a patient positional accuracy in the range of 3 mm to 3.5 mm, which may be insufficient for some cases of stereotactic radiosurgery [27–30]. Therefore, the Gamma Knife Icon™ incorporated the IFMM. This monitoring system consists of an infrared (IR) camera, a reference tool and a patient marker which allow a tracking accuracy of 0.15 mm [23,26,31]. The patient marker is positioned on the nose tip and the movement is detected through four IR reference markers located on the mask holder. There are two different monitoring modes in the IFMM. The first mode is the active mode, in which the treatment is stopped when the IFMM system detects a patient movement exceeding the permissible limits that can be configured from 0.5 mm to 3 mm [23]. The treatment will continue after the patient returns to the original positioning. The second mode is the passive mode, in which warning messages are shown if there are considerable positioning deviations (out of the defined limits) but the dose delivery is not stopped by the system [26]. In this mode, the interruption of the treatment depends on the treating physician or technician.

2.1.5 Leksell Gamma Plan

The Leksell GammaPlan v11.0.3 (LGP) is a treatment planning software for GK units specifically designed to assist physicians and physicists in creating GK treatment plans. The Gamma Knife® Icon™ enables a fast dose planning with high conformity and accuracy by using WarpSpeed and Inverse Planning. The WarpSpeed tool allows to modify, add and remove isocenters (i.e. shots) while providing instant feedback of the dose distribution [32]. This feature allows a considerable reduction in the time required for treatment planning with GK. The Inverse Planning tool [22] has two independent functions: filling and optimization. The filling function allows to estimate a preliminary plan by automatically determining the number of isocenters (i.e. shots) and their positions based on the target volume and on pre-configured treatment quality parameters. The optimization feature allows to improve the preliminary plan by performing a thousand iterations and selecting the plan with the best treatment quality parameters.

The optimization process is determined by four treatment quality parameters, which are coverage, selectivity, gradient index and beam-on time. The coverage parameter represents how much of the target receives the prescribed dose and it is defined as the ratio between the volume in the target region with at least the prescribed dose (VTPD) and the volume of the target region (VT) [33]. The selectivity parameter is used to represent how much healthy tissue is spared and it is defined as the ratio between the VTPD and the total volume receiving at least the prescribed dose (VPD) [33]. The gradient index, which describes the dose fall-off, is another parameter to measure the impact of the treatment in the healthy tissue and it is defined as the ratio between the volume receiving at least half of the prescribed dose ($VTPD_{1/2}$) and the VPD [33]. The beam-on time (BOT) is the sum of the radiation exposure times for every shot defined in the treatment plan [34]. The expected values for these treatment quality parameters are coverage ≥ 0.98, selectivity ≥ 0.85 and gradient index ≤ 3.0. It is an aim of the treatment planning that the BOT is as short as possible for patient comfortability and to avoid motion. In addition, long treatments (above ~ 45 min) could be only delivered using a stereotactic frame while shorter treatments can be delivered also using the thermoplastic mask. However, the decision of using the frame or the mask depends on the treating physician and on the patient's condition.

The LGP system calculates the radiation dose based on the configuration of the GK unit, the geometry of the patient's head and the number, time and collimation of the planned shots. These parameters are essential to analyze the dose distribution and to calculate the dose in every voxel in the regions of interest (ROIs). Generally, in radiotherapy with LINACs, it is intended that the dose be evenly distributed in the target region to prevent cold spots (areas with too low dose) and hot spots (areas with too high dose). However, the dose in the target region in GK radiosurgery is inhomogeneously distributed due to the delivery method. The intended "hotter" regions could experience an enhancement in the cell-killing but could also produce necrosis. Therefore, the prescribed dose and the prescription isodose line limit the dose in the

target region. The system uses mathematical algorithms to calculate the dose in every voxel, which includes the dose contributions from all the shots [35]. There are three algorithms available in the LGP for dose calculation: tissue maximum ratio (TMR), TMR 10 and a CT-based convolution algorithm. Both the TMR classic and the TMR10 considers the head as a uniform water phantom, while the CT-based convolution algorithm considers tissue inhomogeneities in the dose calculations [36].

2.1.6 Treatment Planning Process

Neurosurgeons, radiation oncologists and medical physicists work together to create a patient's treatment plan. A good treatment plan will lead to a short treatment time with high dosimetric quality (considering coverage, selectivity and gradient index). A shorter treatment time is beneficial for the patients as a reduced time improves the comfortability of the patient [37]. For some patients, a reduced treatment time is a must as, due to the patient condition, it is not possible for the patient to stay still or laying on the couch for long periods.

The treatment outcome relies considerably on the contouring of the target region which is critical to achieve the desired local tumor control but also to reduce the normal tissue toxicity [38]. Moreover, tolerance dose limits are defined for the organs at risk (OARs) to avoid normal tissue complications. The size and location of neuroanatomic structures must also be carefully taken into consideration when designing the treatment plan. For example, if a tumor is close to the optical structures (e.g. the chiasm and the optic nerve), the separation between the tumor and such a structure should be at least 4 mm before considering GKRS [24]. In order to minimize the risk of optical neuropathy, the dose to the optical structures should be limited to less than 10 Gy. Therefore, the careful definition and delineation of OARs are essential during treatment planning. Thus, a treatment plan is only accepted if, in addition, to cover the target with the prescribed dose, the dose distribution in the OARs meets the defined criteria to avoid normal tissue complications.

The International Commission of Radiation Units and Protection (ICRU) in its Report 50 (1993) provides a guideline for the physicians to facilitate volume contouring. There are three target volumes typically defined when designing the treatment plan: gross target volume (GTV), clinical target volume (CTV), and planning target volume (PTV), as shown in **Figure 3** below. The GTV is the observable volume of the tumor that can be interpreted as a region of the tumor where the cell density is higher [39]. The CTV is based on the GTV but also includes an additional margin to cover the microscopic disease areas (i.e. regions with tumor cells that cannot be observed in the images) and thus avoid the proliferation of sub-clinical disease. Therefore, treatment including the region contoured by the CTV is essential to achieve cure. Lastly, the PTV is based on the CTV but also includes an extra margin to account for geometric uncertainty due to positioning, for example.
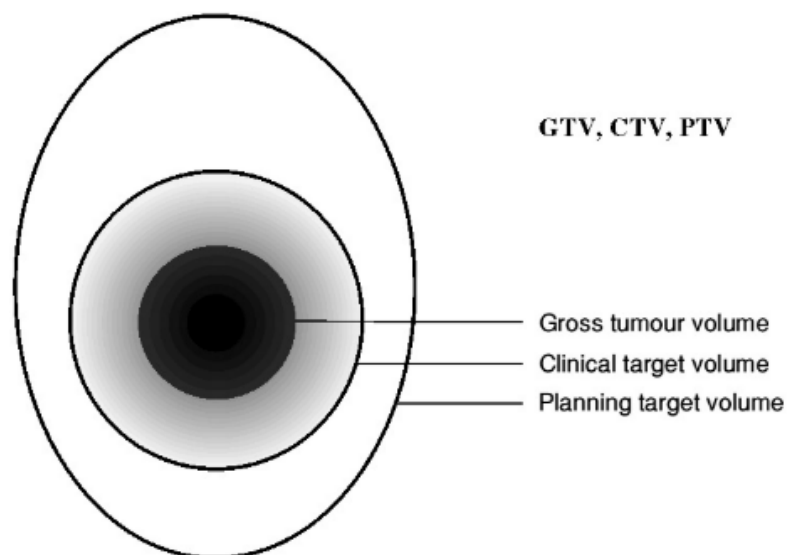
Figure 3 Treatment planning volume definition based on ICRU 50 [39].

There are two main kinds of treatment planning, forward planning and inverse planning. The forward planning method is performed in most clinical environments with gamma knife radiosurgery using a trial and error strategy. Thus, the planner adds and/or removes shots at will and modifies their locations and configurations until achieving the intended dose characteristics for the PTV and the OARs. Although forward planning is time-consuming and the quality of the treatment plan depends on the planner skills, it is still possible to achieve satisfactory plans using forward planning. On the other hand, in inverse planning, the goals of the plan (i.e. dose characteristics for the PTV and the OARs as well as the treatment quality parameters) are given as the input of the treatment planning software and the software delivers the total amount of shots, their location, weight and collimation. Thus, inverse planning allows a faster treatment planning process with better results than forward planning in many cases. The LGP version 10 and above include an inverse planning algorithm which eases the treatment planning process.

In GK radiosurgery, the physical radiation dose is often prescribed to the 50% isodose line. However, the isodose lines used in the prescription can be modified to optimize the dose gradient outside the target depending on the criteria for particular clinical cases [40]. The prescribed physical dose describes the minimum radiation dose received by the tumor and varies for different kinds of tumors. Thus, the maximum tumor dose is twice the prescription dose when the prescription isodose line is 50%. For example, if the patient is prescribed with 12 Gy at the 50% isodose line, the maximum dose within the tumor will be 24 Gy (100%). The prescribed physical dose is based on the tumor volume, the primary tumor histology and prior treatment. The tumor volume needs to be considered in the prescribed dose as potential adverse effects are proportional to the irradiated tumor volume [5]. In addition, the prescription dose also varies depending on the type of tumor.

2.1.7 Clinical Workflow GK Radiosurgery

The clinical workflow with GK starts with the definition of the head immobilization device, frame or mask, depending on the patient condition and the tumor characteristics (i.e. type, shape, location and size). The Leksell stereotactic G-frame (Elekta Instrument AB, Sweden) consists of four fixation pins, four support posts, and the base ring of the frame. For the GK Icon, there is a mechanical frame adapter between the frame and the treatment couch. The frame-based fixation is inappropriate for fractionated treatment due to the invasiveness of the frame. On the other hand, the thermoplastic mask (ICON™ Nanor) is made of a nanoparticle compound which was specially designed for molding at low temperatures (62.8 ºC [145 ºF] and higher) [41]. The main attribute of this mask is to improved patient comfort while ensuring a high precision treatment delivery. Unlike with frame-based fixation, multisession GK radiosurgery becomes possible with the mask-based fixation. In general, frame-based fixation, which allows a more accurate positioning with less motion, is used for single-fraction treatments with longer treatment times or with targets near critical anatomical structures. Mask-based fixation (with thermoplastic mask) is used for single-fraction or fractionated treatments, usually with shorter treatment times and no critical structures around to the targets or when the patient cannot tolerate the use of the frame.

The frame-based procedure is usually initiated with the acquisition of an MR scan, which offers superior soft-tissue contrast, for diagnosis and contouring of the regions of interest one or two days before the treatment delivery. On the treatment day, the patient receives local anesthesia at the sites of the head where the frame pins will be placed. The Leksell "G-frame" is mounted on the patient head by a physician using a 4-point fixation with a torque of approximately 30 cNm [42]. The placement of the frame is crucial as the main target needs to be as close as possible to the frame centroid while achieving a stable frame attachment. The frame has built-in 3D coordinate scales which help with the frame positioning. After the frame is mounted, the patient undergoes regular diagnostic CT scanning in which an "indicator" box is placed to generate fiducial marks in the images. The CT images are used to define the reference for the stereotactic coordinate system and to apply radiation attenuation correction during treatment planning. The stereotactic coordinate system from the CT scan and the stereotactic space in the LGP treatment planning system are co-registered by selecting the fiducial marks that emerge in the CT image because of the presence of stereotactic "indicator" box. The CT image is then co-registered with the MR image in the LGP treatment planning system for precise target localization and the treatment plan is finalized. Before treatment delivery, the patient is set up on the GK couch with the head precisely positioned for treatment using the stereotactic frame. Then the treatment is delivered, which lasts between 20 min and 2 h and during which the patient does not experience any pain produced by the radiation treatment. Once the treatment is completed, the head frame is removed.

Similar to the frame-based workflow, the frameless workflow (i.e. using the thermoplastic mask) also starts with an MR scan one or two days before treatment

delivery. Subsequently, the patient's mask is created. The nose part of the mask is trimmed to place a single reflective optical marker on the tip of the patient's nose. This marker serves as an anatomical reference for motion monitoring during treatment delivery. The patient then undergoes a standalone CBCT scan for stereotactic referencing. Optionally, the patient also undergoes CT scanning with the mask on for better attenuation correction. The MR, CT, and CBCT images are then co-registered in the LGP treatment planning system for target localization and verification. The treatment plan is finalized and sent to the Gamma Knife unit. A CBCT scan is performed again to confirm patient positioning before the delivery of the treatment. Once the patient positioning is confirmed, the treatment is delivered. For fractionated treatment, a CBCT scan is performed before each fraction to ensure positional accuracy for each treatment fraction.

2.2 Brain Tumors

Uncontrollable and abnormal growth of brain cells leads to the occurrence of benign or malignant brain tumors. The initial site of occurrence can be either in the brain itself (i.e. primary brain tumor) or in other parts of the body from where the tumor cells spread to the brain (i.e. brain metastasis). Brain tumors can be classified as benign tumors (i.e. tumors that do not spread out of the primary site) or malignant tumors (i.e. tumors which can spread to neighboring tissues or to other parts of the body). Some examples of benign tumors are vestibular schwannoma, pituitary adenoma and most meningiomas while brain metastases and glioma are the most representative cases of malignant tumors, also called cancerous tumors.

Brain metastases (BMs) are found in up to 20% - 40% of cancer patients [43,44] and are commonly produced from primary cancer in the lungs, breast, skin (melanoma), colon and kidneys. The type of cells in the brain metastases is usually similar to the cells in the primary site of the tumor. Single or multiple brain metastases can be found, depending on the aggressiveness of primary cancer. The treatment options for patients with brain metastases are surgical resection of the tumor(s), whole-brain radiation therapy (WBRT), radiosurgery or a combination of these modalities. The combination of surgery and WBRT has improved patient survival rates and local tumor control for the patient with few brain metastases [45,46]. However, depending on the size and location of the brain metastases, surgery is not always possible [47,48]. Alternatively, some studies have shown that the combination of radiosurgery and WBRT improves patient's quality of life and survival compared to only WBRT [49] and that radiosurgery alone results in high rates of tumor response and local control [50–52]. In addition, Yamamoto et al. showed that radiosurgery alone can be effective to treat patients with up to ten brain metastases [53].

Another aggressive malignant brain tumor produced from glial cells is known as glioblastoma multiforme (GBM). GBM usually occurs in adults (40-70 years old) and constitutes about 15% among all brain tumors [54,55]. The location of the tumor in the brain determines the symptoms of patients with GBM. GBM patients may suffer from

headaches, seizures, nausea and vomiting, changes in vision, loss of appetite, changes in mood and behavior, concentration deficit, and motor or sensory deficiency [55]. Patients with GBM are usually treated with surgery, radiation therapy and chemotherapy. Surgical resection followed by radiation therapy is considered as the standard management for GBM patients [56]. GK radiosurgery is often used as adjuvant therapy after surgery or for tumor recurrence in GBM patients. However, the efficacy of GK radiosurgery for GBM has not been clearly demonstrated [56], although Larson et al. showed an improved survival rate for treatments combining GK radiosurgery with other therapeutic modalities [57].

Different to brain metastases and GBM, meningiomas are mostly benign non-cancerous tumors which originate in the inner layer of the meninges. However, approximately 10% of meningiomas are malignant. These kinds of tumors are difficult to remove surgically as they grow in between the bottom of the skull and the back of the eyes. The symptoms of patients with meningioma depend on the tumor size and location. Meningioma patients usually experience a loss of sensitivity in the arms or legs as well as other symptoms such as headaches, seizures, vision problems and weakness. Approximately 80%-100% of the meningioma cases can be controlled with radiosurgery [58]. Thus, Gamma Knife therapy represents a useful alternative for patients with meningioma, especially for tumors located near essential structures in the brain, which complicates a surgical treatment. Meningiomas with sizes of 4 cm or smaller respond better to treatment with Gamma Knife [58].

Pituitary adenomas, benign tumors of the anterior pituitary gland caused by a hormonal imbalance, account for 10% to 15% of all intracranial tumors [59]. The symptoms produced by a pituitary adenoma depend on the tumor type and on the area of the pituitary gland affected. These kinds of tumors are treated with medication, surgery, radiotherapy and stereotactic radiosurgery. Surgical resection of the tumor results in a decrease of the neurological symptoms [60], but this is not feasible when the tumor infiltrates the cavernous sinus. However, there is a 20% to 50% possibility of tumor recurrences after surgery [61–63]. Alternatively, it has been proven that the size of pituitary adenoma can be effectively controlled using GK radiosurgery with a rate of tumor control higher than 90% [59,61,64–66].

Vestibular schwannomas (VS) or acoustic neuromas are uncommon and benign tumors originated from the Schwann cells (cells of the peripheral neural system that allow the fibers of the peripheral nerves to live) [67]. The incidence of vestibular schwannomas is about 1 in 100 000 people. The growth of vestibular schwannomas is usually slow, and their detection is possible when they have a considerable mass or when they produce compression of the proximal cranial nerve. Patients with vestibular schwannoma may experience hearing problems, loss of sensitivity in the face, weakness, ear pain and changes in the gustatory perception. Vestibular schwannoma is managed through observation, resection, radiotherapy (fractionated) and stereotactic radiosurgery to control the tumor growth, to preserve hearing and to protect the facial nerve [3]. For larger VSs, resection is the preferred choice as it reduces

the mass effect on the brainstem. However, surgical resection usually requires adjuvant treatment as the rate of recurrence increases with the size of the VS. Multiple studies have shown the efficacy of stereotactic radiosurgery in managing VS (small and medium-size) [68–72]. The cochlear dose during radiosurgery is crucial for hearing preservation. According to a study on 38 VS patients treated with SRS, the hearing function deteriorates in patients who receive a higher minimum cochlear dose during treatment [73]. Therefore, it is crucial to contour and consider the dose to the cochlea during treatment planning [74].

The disorder of the fifth cranial nerve causing facial pain is known as trigeminal neuralgia (TN). In some patients, TN is accompanied by some atypical characteristics such as burning, chronic pain or severe pain [75]. The efficacy of GK radiosurgery in managing patients with TN has been proven in multiple studies, especially in patients for whom surgery is not possible [65,76,77]. As in other radiosurgery treatments, it is essential to accurately delineate all proximate critical structures (i.e. brainstem, optical apparatus and cranial nerve) and to consider the radiation dose in them during treatment planning to avoid radiation adverse effects [77].

2.3   Radiobiology of Radiosurgery

The gamma rays from the ^{60}Co sources are absorbed in the tissues via the Compton effect which is producing fast electrons. The Compton effect is the interaction of photons with charged particles in matter that produces a loss of energy in the photons, which is transferred to the charged particles and may result in the emission of electrons from the outer energy shell of the atoms. The fast electrons produced by the ^{60}Co irradiation cause tissue damage in two ways: indirect damage (the electrons interact with the water molecules around the DNA and produce hydroxyl radicals that can damage the DNA by breaking the DNA chemical bonds) and direct damage (the electrons interact directly with the DNA resulting in single- or double-strand breaks) [78]. The amount of strand breaks in the DNA is an indication of the loss of biological functions produced in tissues or cells.

The radiation damage produced in the DNA is classified as potentially lethal damage and sublethal damage. The repair of potentially lethal damage is in principle not possible and produces cell death. In contrast, sublethal damage can be repaired and usually occurs within 24 h after irradiation, except if the damage is more pronounced than the repair rate in the cells. The most common mechanism of cell death is mitotic death, where cells will not die until they try to reproduce. Mitotic death describes the process of cells to divide before they die because of chromosome damage. This implies that the biological effects of irradiation, such as tumor shrinkage, may take days, months, or even years to appear depending on how fast the replication of cells is. In addition, apoptosis, or programmed cell death, is another mechanism leading to cell death that usually occurs in healthy cells after irradiation.

The tumor growth is typically slow and decreases after irradiation as the tumor cells are unable to rapidly repair the DNA damage produced by the irradiation. Differently to cancerous cells, most normal cells (late responding tissue) appear to recover more effectively after irradiation when receiving the same radiation dose. The biological impact depends considerably on the type of irradiated tissue, more specifically on its radiation sensitivity, and on the absorbed dose. Usually, tumor cells are more radiosensitive and take longer to repair the DNA damage than normal tissue, which allows fractionated radiotherapy treatment. Late responding tissues are much more susceptible than acute-responding tissues to a fractionated radiotherapy scheme [79]. Irradiation of serial organs (usually with a small transversal area in which the functional continuity of the organ is important, such as nerves) produces a different biological effect than irradiation of parallel organs (the continuity of the organ is not important, only the affected volume) [6]. Therefore, the kind of organ (serial or parallel) needs to be considered to better determine the biological effect in the organs after irradiation.

2.3.1 Cell Survival Curve

Clonogenic cells are cells that have the reproductive capability and therefore can proliferate [78]. The alteration of the reproductive control genes in clonogenic cells can lead to uncontrolled growth that producing high accumulation of cells (i.e. tumors). Therefore, to sterilize a tumor, the objective is to kill or inactivate all its clonogenic cells. Thus, the tumor proliferation and overall effect of irradiation on the tumor depends on the number of clonogenic cells surviving after radiotherapy. The cell survival is determined by the received absorbed dose. The plot of the absorbed radiation dose against the proportion of cells that survive after irradiation is known as a cell survival curve [78]. The cell survival after irradiation can be partially described by an exponential function and is usually plotted on a logarithmic scale, which facilitates the interpretation of the curve, especially to observe the effect for low survival rates. A typical cell survival curve is presented in **Figure 4** below.
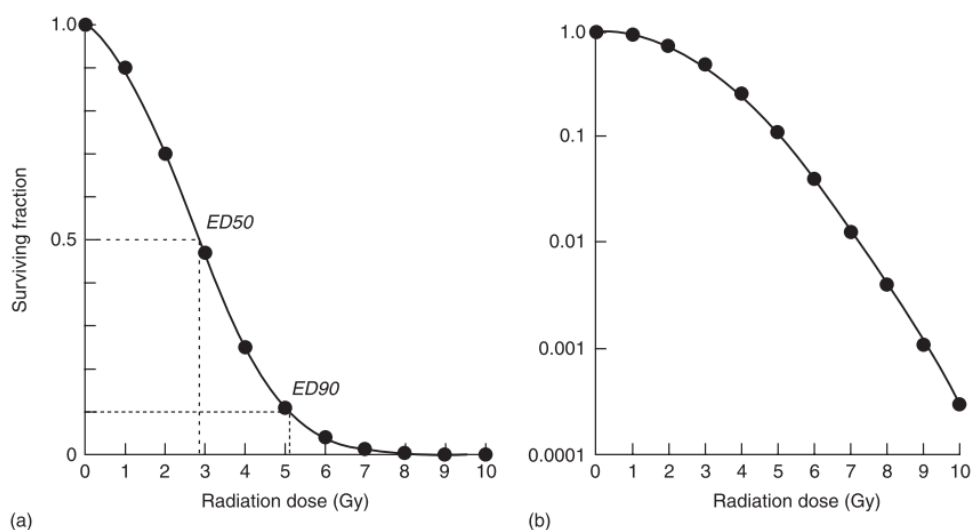
Figure 4 A typical cell survival curve for cells irradiated in tissue culture. (a) linear scale (b) the same data plotted on logarithmic scale [80].

2.3.2 Linear Quadratic Model

The linear-quadratic (LQ) model is the most commonly used model for analyzing the survival response of cells after irradiation [3]. The LQ model determines the fraction of cells that survive after irradiation by considering two forms of DNA damage expressed by a linear term (used to described lethal damage) and a quadratic term (used to describe sublethal damage, which allows DNA repair) [81]. Based on the LQ model, the survival fraction (SF) is expressed as:

$$SF = exp^{(-\alpha D - G\beta D^2)} \tag{1}$$

where D is the absorbed dose (Gy) and α (Gy^{-1}) and β (Gy^{-2}) are the linear and quadratic tissue radiosensitivity parameters, respectively.

The linear coefficient α (Gy^{-1}) describes the initial part of the survival curve and accounts for the non-repairable DNA damage which kills the cells by a single radiation event (lethal damage). The quadratic component β (Gy^{-2}) describes the late section of the survival curve and represents the DNA damage that requires multiple radiation hits to produce cell death, which may be repairable with time (sublethal damage). The G factor also called the Lea-Catcheside dose-protraction factor, describes the relationship between dose rate, repair rate, absorbed dose and exposure time [82,83]. The G factor is expressed as:

$$G(T) = \frac{2}{D^2} \cdot \int_0^T \dot{D}(t) \cdot \left(\int_0^t \dot{D}(w) \cdot e^{-\mu_{rep} \cdot (t-w)} \cdot dw \right) \cdot dt \tag{2}$$

where T is the radiation exposure time, t and w are integration time variables, and D, $\dot{D}(t)$ and μ_{rep} are the absorbed dose, dose rate at time t and the cell repair rate, respectively. The G factor is assumed to be 1 for acute absorbed doses, as in external beam radiotherapy with LINACs.

2.3.3 Biological Effective Dose

Barendsen first introduced the concept of BED in 1982 from the concept of extrapolated tolerance dose (ETD), which was later renamed as extrapolated response dose (ERD), and finally received the name of biologically effective dose (BED) by Fowler [84,85]. The BED is a representation of the absorbed dose which considers the biological effect produced in the tissues by the irradiation. Based on the LQ model, the BED is defined as:

$$BED = D \cdot \left(1 + \frac{G}{\alpha/\beta} \cdot D \right) = -\frac{ln(SF)}{\alpha} \tag{3}$$

where the α/β ratio (Gy) is the tissue-specific radiosensitivity towards a particular type of ionizing radiation. Tissues or cells with a higher α/β ratios are more sensitive to ionizing radiation. The α/β ratio also describes the dose value at which the linear contribution to the cellular damage (αD) is equal to the quadratic contribution (βD^2). Thus, the α/β ratio (Gy) can be defined as:

$$\alpha D = \beta D^2 \tag{4}$$

$$D = \alpha/\beta \tag{5}$$

The α/β ratio is the most influential radiobiological parameter in the BED formula as it allows to differentiate the types of tissues (early or late responding tissues). Higher α/β values (e.g. 10 Gy) are characteristic of early responding tissues and most tumors while lower values (around 2 Gy or 3 Gy) are used for late responding tissues. A subscript with the α/β ratio value is added next to the absorbed dose unit (Gy) to represent the units of BED which avoid any confusion when comparing BED values (e.g. a unit of Gy_{10} is used if the BED was calculated with an α/β ratio of 10 Gy). The subscript in the unit also indicates that the value corresponds to a biological dose, and not to a physical dose.

The BED value is indeed an indicator of the biological effect in the tumors and normal tissue. Thus, higher BED values indicate a higher biological effect. Tissues with smaller α/β ratios (late responding tissues) have a more significant repair effect compared to tissues with larger α/ß ratios (early responding tissues). Hence, the survival fraction is higher in late responding tissues compared to early responding tissues.

The BED depends on the dose rate and the exposure time, which implies that periods of no irradiation contribute to reduce the total biological effect after radiotherapy. Thus, the use of BEDs instead of absorbed doses during treatment planning may lead to improved radiation treatment protocols with better therapeutic ratios (i.e. ratio between tumor BED and OAR BED). In addition, some of the clonogenic tumor cells would survive, repair and repopulate, which in turn reduce the efficacy of the treatment. Therefore, it is of high importance to include repair components in the measurement parameter to determine the efficacy of radiation treatment.

The standard BED equation, however, needs an adjustment to account for incomplete repair by considering the two-hit damage where the two hits are in different fractions. The values of BED with incomplete-repair are always higher compared to non-repair-corrected BED values. Therefore, a comparison cannot be made between BED values corrected for repair and non-corrected repair BED values [86].

3 MATERIALS AND METHODS

3.1 Patients

A group of 25 patients with various brain tumors treated with GK radiosurgery at the Department of Radiation Oncology, University Medical Center Mannheim, Germany between 2015 and 2019 were retrospectively selected for analysis in this thesis work. **Table 1** below illustrates the tumor type and the GK treatment characteristics for each patient selected for this analysis.

Table 1 Tumor type and GK treatment characteristics for analyzed patients.

Patient ID	Tumor type	Target Volume (cc)	Prescribed dose (Gy)	Prescription isodose line (%)	No. of Shots
[1]Pt 1	VS	0.24	12	50	6
[1]Pt 2	VS	0.29	12	65	6
[1]Pt 3	VS	0.19	12	65	7
[1]Pt 4	VS	0.14	12	50	4
[1]Pt 5	VS	0.72	12	50	7
[1]Pt 6	Glio	0.20	16	50	7
[1]Pt 7	Glio	0.62	6	50	6
[1]Pt 8	PA	0.16	25	50	5
[1]Pt 9	MET	0.36	16	70	4
[2]Pt 10	Glio	0.28	16	50	5
[2]Pt 11	MEN	0.18	16	50	6
[2]Pt 12	MEN	0.27	16	50	7
[2]Pt 13	MET	0.85	22	50	6
[2]Pt 14	MET	0.28	22	50	5
[2]Pt 15	MET	0.57	16	50	6
[2]Pt 16	MET	0.91	22	50	5
[2]Pt 17	MET	1.18	22	50	4
[2]Pt 18	MET	2.42	22	50	5
[2]Pt 19	MET	2.08	22	50	4
[2]Pt 20	MET	0.63	22	50	5
[2] Pt 21	MET	27.41	10	50	17
[2] Pt 22	MET	14.43	8	50	20
[2] Pt 23	MET	10.40	10	50	25
[2] Pt 24	MET	7.78	16	50	27
[2] Pt 25	MET	10.52	20	50	33

[1]Pt = patient with OAR(s) delineated for treatment planning.
[2]Pt = patient with no OAR delineated for treatment planning.
VS = Vestibular Schwannoma, Glio = Glioblastoma, PA = Pituitary Adenoma,
MEN = Meningioma and MET = metastasis (single target only)

The treatment plans for all patients were generated using the Leksell Gamma Plan (LGP) version 11.0.3 and the patients were treated with the Gamma Knife® Icon™. The number of shots ranged from 4 to 33 (median of 6), and the mean target volume was 3.3 cc ± 6.4 cc (median of 0.62 cc, range from 0.14 cc to 27.41 cc). The mean prescription dose to the target was 16.2 Gy ± 5.3 Gy (median of 16 Gy, range from 6 Gy to 25 Gy), and the prescription isodose lines varied from 50% to 70%.

3.2 Ethics Statement

This study received approval from the Medical Ethics Commission II (Medizinische Ethik - Kommision II), Medical Faculty Mannheim, Heidelberg University (2015-621N-MA) and was conducted according to the tenets of the Declaration of Helsinki. Written consent was waived due to the utilization of anonymized imaging data with no personal information.

3.3 Radiobiological Simulations and Processing

3.3.1 Data extraction

The data extraction process started with the isolation of each shot by setting the weights of all other shots to zero. All other settings were fixed similarly to the clinical treatment plan. The dose prescription was adjusted until the shot beam-on time was equal to the beam-on time of the shot in the clinical treatment plan. Thus, the single isolated shot will produce the same dose distribution with the same dose rate per voxel as when integrated into the actual clinical plan. The 3D dose distributions produced by every single shot were exported as Digital Imaging and Communications in Medicine (DICOM) files conserving the same dose grid and resolution. The CT images used for treatment planning as well as the contoured structures (PTV and OARs), and the treatment plans (clinical plan and the plans for each isolated shot) were also exported as DICOM files. The treatment plan DICOM files contain information about the sequence of shots as well as the dose rate, the total delivered dose, and the beam-on time for each shot. The clinical treatment plan was used as a reference to measure the improvement achieved by modifying the shot sequence.

The dicomrt-toolbox-v2 from Computational Environment for Radiological Research (CERR) [87] was used in conjunction with MATLAB 2018a, The MathWorks, Inc., Natick, Massachusetts, United States to retrieve all the information from the DICOM files exported from the GK treatment planning system (i.e. CT images, treatment plans, structures, and dose distributions). A hierarchical MATLAB structure was created for each patient with the retrieved information to allow automated processing. MATLAB® 2018a was also used for all the other calculations required for the data analysis.

The retrieved absorbed doses, dose rates, dose distributions and beam-on times of each planned shot were used to determine the impact of the shot sequence on the treatment efficacy for the analyzed treatment plans [88]. Improvement in the treatment

efficacy was determined by the variation in the therapeutic index (for patients with defined OARs) or in the tumor BED (for patients without defined OARs).

3.3.2 Permutation of the shot sequence

Different combinations of the shots were analyzed to determine the shot sequence with the best therapeutic characteristics (i.e. higher therapeutic index or higher tumor BED). The total number of possible shot sequences depends on the amount of planned shots and is equal to the factorial of the number of shots. For example, a treatment plan consisting of 4 shots will produce 24 (i.e. 4!) possible shot combinations while for a plan with 10 shots 3 628 800 (i.e. 10!) possible sequences exist. A permutation function in MATLAB (perms.m) was used to produce all the possible shot sequences for patients with treatment plans with 10 or less shots. Due to the high computational processing and required memory, only 1000 randomly generated shot sequences were analyzed for patients with treatment plans with more than 10 shots.

3.3.3 Biological effective dose calculation

BED values were calculated for each voxel in the target volume and in the delineated regions for the OARs, if available, for all the evaluated shot sequences. Additionally, the effect of incomplete repair was considered in the BED calculations by using three different repair models. The three repair models analyzed in this work were: mono-exponential repair model (R_{ME}), reciprocal repair model (R_{RR}) and bi-exponential repair model (R_{BE}) [89]. Thus, BED considering incomplete repair was then calculated as follows:

$$\text{BED} = D\left[1 + \frac{1}{D\left(\frac{\alpha}{\beta}\right)}\sum_{i=1}^{N}\sum_{j=1}^{N} d_i d_j R\big(|S_i - S_j|\big)\right] \tag{6}$$

$$R_{ME}(t) = \exp\left(-\frac{t}{\tau}\right) \tag{7}$$

$$R_{RR}(t) = \frac{1}{1 + t/\tau} \tag{8}$$

$$R_{BE}(t) = \varepsilon \cdot \exp\left(-\frac{t}{\tau_1}\right) + (1 - \varepsilon) \cdot \exp\left(-\frac{t}{\tau_2}\right) \tag{9}$$

where D is the total absorbed dose, N is the number of shots, d_i is the fractional dose (i.e. dose contribution) produced by the i-th shot (i = 1….N), d_j is the fractional dose produced by the j-th shot (j = 1….N), α/β is the tissue-specific radiosensitivity, S_i is the starting time of the i-th shot and S_j is the starting time of the j-th shot. For the mono-exponential repair model (Eq. 7), and the reciprocal repair model (Eq. 8), τ is the repair

halftime while for the bi-exponential repair model (Eq. 9) τ_1 and τ_2 are the fast and slow repair halftimes, respectively. The epsilon (ε) in Eq. 9 is the partition coefficient between the fast and the slow repair components (with $0<\varepsilon<1$). The term $|S_i - S_j|$ (i.e. time difference between shots) in Eq. 6 corresponds to t in equations (7, 8 and 9).

For a very fast repair with equal dose contribution from all shots, the repair term R becomes the unity for j=i and zero otherwise. Thus, the double sum component in Eq. 6 becomes equal to Nd^2, and Eq. 6 becomes Eq. 10, which is the BED equation usually applied for fractionated external beam radiotherapy (EBRT).

$$BED = Nd\left(1 + \frac{d}{\alpha/\beta}\right) \tag{10}$$

On the other hand, for a very slow repair and equal dose contribution from each shot, R becomes 1 for all values of i and j. Hence, the double sum component in Eq. 6 becomes equal to N^2d^2, and Eq. 6 becomes Eq. 11, which is equivalent to the BED equation for a single fraction treatment in EBRT (replacing Nd by D):

$$BED = Nd\left(1 + \frac{Nd}{\alpha/\beta}\right) \tag{11}$$

To obtain optimal tumor control probability and avoid necrosis, in EBRT it is traditionally intended that the dose distribution in the target volume is as uniform as possible, avoiding cold spots (i.e. regions with less than 95% prescribed dose) and hot spots (i.e. regions with more than 107% prescribed dose) [90]. However, in Gamma Knife radiosurgery the dose distribution is not homogeneous due to the effect of the cumulative dose from each shot in every voxel. Thus, the target volume is divided into N sub-volumes (N = number of voxels in the target region) to account for the non-uniform dose distribution in the calculation of the BED. The dose distribution within each voxel was assumed uniform to calculate the BED for each voxel. Subsequently, the overall biologically effective dose (oBED), which determines an effective BED for inhomogeneous dose distributions, was used to calculate the effective biological dose in the entire target volume and in the OARs [91]. The oBED was calculated as follows [91]:

$$oBED = -\frac{1}{\alpha} \cdot ln\left[\frac{1}{N}\sum_{i=1}^{N} exp(-\alpha.BED_i)\right] \tag{12}$$

where α is the linear parameter in the LQ model, N is the number of voxels in the region of interest (target volume or OAR), and BED_i is the BED for each voxel calculated with Eq. 6 with each of the analyzed repair models (Eq. 7, Eq. 8 and Eq. 9).

The radiobiological parameters used for the calculation of BED for each voxel for the oBED calculation are shown in **Table 2, Table 3** and **Table 4.**

Table 2 Radiobiological parameters used in the BED calculations with a mono-exponential repair model [18,92].

Parameter	Tumor	Normal tissue
α/β (Gy)	10	2.47
α (Gy^{-1})	0.06	0.07
Repair halftime (h)	0.5	1.5

Table 3 Radiobiological parameters used in the BED calculations with a reciprocal repair model [18,92,93].

Parameter	Tumor	Normal tissue
α/β (Gy)	10	2.47
α (Gy^{-1})	0.06	0.07
Repair halftime (h)	0.5	2.8

Table 4 Radiobiological parameters used in the BED calculations with a bi-exponential repair model [18].

Parameter	Tumor	Normal tissue
α/β (Gy)	8.31	2.47
α (Gy^{-1})	0.241	0.07
β (Gy^{-2})	0.029	0.03
Fast repair halftime (h)	0.13	0.19
Slow repair halftime (h)	1.34	2.16
Partition coefficient (ε)	0.20	0.98

3.4 Selection of the optimal shot sequence

For patients whom OARs were delineated, the shot sequence leading to the highest therapeutic index (i.e. the ratio between the target oBED and the oBED for the dose-limiting organ) was selected as the optimal shot sequence while for patients with no defined OARs, the shot sequence leading to the highest target oBED was defined as the optimal sequence. For patients with more than one defined OAR, the dose-limiting organ was determined by multiplying the therapeutic index (TI) considering each OAR by the OAR tolerance absorbed dose TD$_{50/5}$ (i.e. the absorbed dose which may produce a 50 % probability of severe normal tissue complication within 5 years after

irradiation) [94]. Thus, the organ with the lowest product between the therapeutic index and the $TD_{50/5}$ was selected as the dose-limiting organ. Although the therapeutic indices were calculated based on BED values, tolerance absorbed doses ($TD_{50/5}$) were used to determine the dose-limiting organ as tolerance values in terms of BED are rarely found in the literature. However, as the BED is directly related to the absorbed dose, the method used to determine the dose-limiting organ can be assumed acceptable for the purposes of this work. Tolerance absorbed doses (also called dose constraints) for OARs relevant in GK radiosurgery are presented in **Table 5**.

Table 5 Tolerance absorbed doses $TD_{50/5}$ for OARs relevant in GK radiosurgery.

Organ	Tolerance dose ($TD_{50/5}$) (Gy)
Cochlear [95]	70
Trigeminal nerve [96]	40
Inner ear [97]	53.6
Cochlea nerve [96]	40
Brainstem [95]	65
Medulla [95]	65
Chiasma [95]	65
Pituitary gland [97]	60.5

The relative change in the therapeutic index (or in the target oBED) between the optimized sequence and the clinical sequence was used to quantify the improvement in the treatment efficacy when the optimized sequence is applied. The relative change was calculated as:

$$\% \; change = 100 \times \left(\frac{TI\_optimal\_sequence - TI\_clinical\_sequence}{TI\_clinical\_sequence} \right) \quad (13)$$

The relative change in the target oBED can be also calculated using Eq. 13 by replacing the TI values with target oBED values.

In this work, the radiobiological effectiveness of the GK treatment is represented by the therapeutic index of each plan (for patients with defined OARs) or by the target oBED values (for patients with no OAR defined). Thus, changes either in the therapeutic indices or in the target oBED values are referred as changes in the radiobiological effectiveness of the GK plan.

3.5 Effect of the decay of the GK sources on the BED

The dose rate of the GK unit depends on the activity of the ^{60}Co sources ($T_{1/2}$ = 5.26 years) and decreases with the decay of the ^{60}Co sources. Therefore, the use of older sources (with lower activity) to generate a treatment plan with the same dose

deposition per shot as a treatment plan generated with newer sources (with higher activity), will produce shots with longer beam-on times and lower dose rates. Thus, to compensate for the effect of the dose rate reduction, the beam-on time for each shot is doubled when the sources are decayed by one half-life [16]. The reduction of the dose rate and the longer exposure times may affect the biological effectiveness of the GK treatment as the probability of sublethal damage repair increases both in the OARs and in the target. Therefore, to analyze the influence of the decay of the GK sources on the biological effectiveness in GK radiosurgery, oBED values for the target were calculated assuming that the GK sources were decayed by one half-life. To simulate the decayed sources conserving the same dose distribution, the dose rates in the original treatment plan were halved while the beam-on times were doubled for each shot. All other parameters in the treatment plan as well as the radiobiological parameters for the oBED calculations remained unchanged. Similarly, as in the analysis of the optimal shot sequence, oBED values were calculated using the mono-exponential repair model, the reciprocal repair model and the bi-exponential repair model. Subsequently, the target oBED values for the clinical plans and the target oBED values for the plans with the decayed sources were compared using the relative change between them as follows:

$$\% \ change = 100 \times \left(\frac{oBED_{decayed} - oBED_{clinical}}{oBED_{clinical}} \right) \tag{14}$$

3.6 Statistics

Descriptive statistics was presented using mean and standard deviation values. Minimum and maximum values were used to present ranges, while the median was used to show typical values.

4 RESULTS

The results obtained after the performed simulations are divided into three sections according to the repair model used for the oBED calculations: mono-exponential repair, reciprocal repair and bi-exponential repair. In each of these sections, patients are categorised into two sub-groups according to the delineated ROIs in their treatment plans. The first sub-group comprises patients with defined OARs (nine patients), while the second sub-group comprises patients with no OAR defined (16 patients). For patients with defined OARs, the impact of using the optimal shot sequence (i.e. sequence with the highest therapeutic index) is presented as changes in the therapeutic indices and in the oBED values both for the target and for the dose-limiting OAR. Moreover, for patients with no OAR defined, the evaluation was made only considering the target oBED values. The clinical sequence is used as a reference in the assessment of all the simulated scenarios. The same grouping method is used to present the results obtained from the simulations in which the GK sources were assumed to be decayed by one half-life when compared to the activity of the sources used in the actual clinical plan.

4.1 Therapeutic effect of using the optimal shot sequence and a mono-exponential repair model

4.1.1 Patients with defined OARs

The therapeutic indices (TIs) for the clinical and the optimal sequences for the nine patients with defined OARs are shown in **Figure 5**. These values as well as the relative change between them are presented in **Table 8** (Appendix). The therapeutic indices for the optimal sequences were higher than for the clinical sequences in all patients. The TI relative change between both sequences ranged from +0.2% to +10.0% (median +3.2%, mean +4.2% ± 3.3%). Patient 7 showed the lowest change (+0.2%), while patient 6 showed the highest change (+10%).
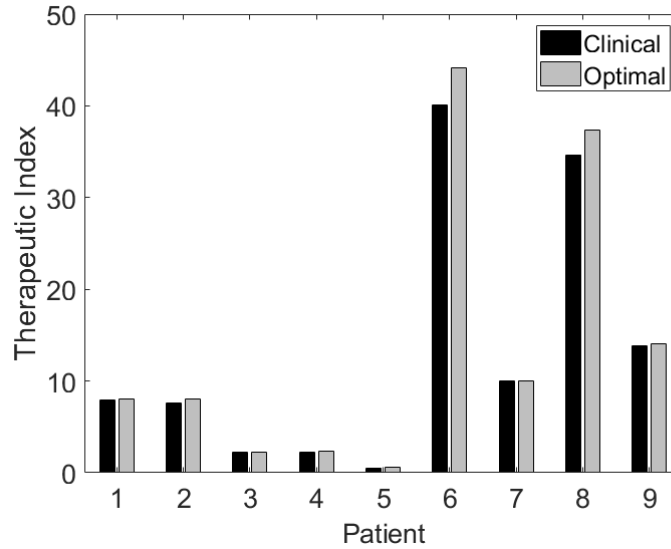
Figure 5 Therapeutic index values for the clinical and the optimal shot sequences (i.e. shot sequence with the highest therapeutic index) for the nine patients with defined OARs. The oBED values used to calculate the therapeutic indices were calculated using the mono-exponential repair model. The therapeutic indices for the clinical and the optimal sequences are shown in black and grey, respectively.

The oBED values for the target and the dose-limiting OAR for the clinical and optimal shot sequences for the nine patients with defined OARs are illustrated in **Figure 6** and also presented in **Table 9** (Appendix). For the target, the mean relative change between the clinical and the optimal oBED values was +5.7% ± 5.9% (median 4.0%, range from -0.2% to +19.7%). The optimal target oBED values were higher than the clinical target oBED values for all patients, except for patient 7 (-0.2%). Moreover, for the dose-limiting OAR, the mean relative change between the clinical and the optimal oBED values was -0.5% ± 2.3% (median 0.0%, range from -4.4% to +2.9%). Five of the nine patients presented optimal OAR oBED values higher than the clinical OAR oBED values. Patient 5 showed a marginal change (+0.002%) between the clinical and the optimal oBED values.
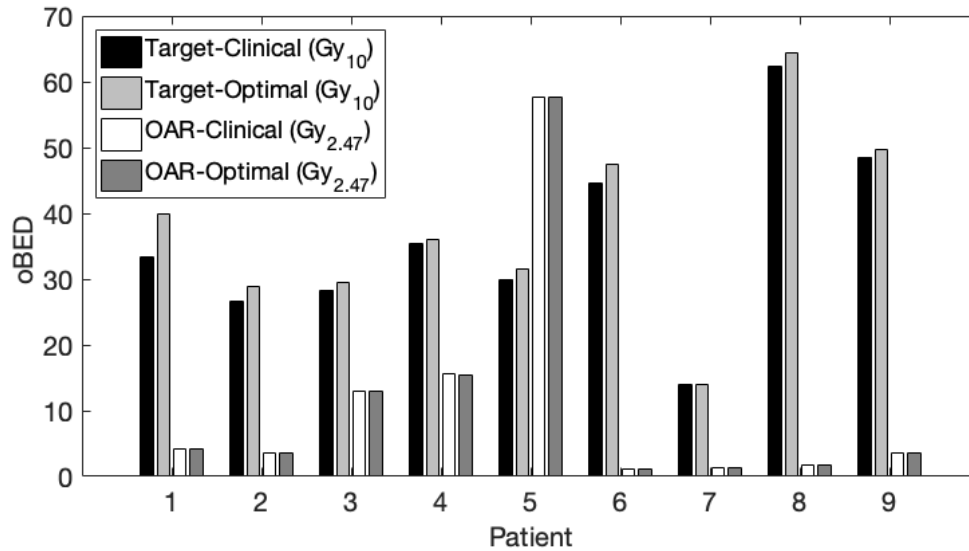
Figure 6 Clinical and optimal oBED values for the target and the dose-limiting OAR for the nine patients with defined OARs. The optimal sequence was defined as the shot sequence producing the highest therapeutic index. The oBED values were calculated using the mono-exponential repair model (α/β = 10 Gy for the target and α/β = 2.47 Gy for the dose-limiting OAR). For the target, clinical and optimal oBED values are shown in black and light grey, respectively. For the dose-limiting OAR, clinical and optimal oBED values are shown in white and dark grey, respectively.

4.1.2 Patients with no defined OAR

Figure 7 shows the comparison of the target oBED values between the clinical and the optimal sequences for 16 patients with no OAR defined. The target oBED values for the clinical sequences and the optimal sequences as well as the relative changes between them are summarized in **Table 10** (Appendix). The target oBED values for the optimal sequences were higher than those for the clinical sequences for all the patients. The relative change between the clinical and the optimal sequences were within +1.6% and +12.1% (median +3.9%, mean +4.3% ± 2.6%). The lowest and highest changes were observed for patient 25 (+1.6%) and patient 12 (+12.1%), respectively.
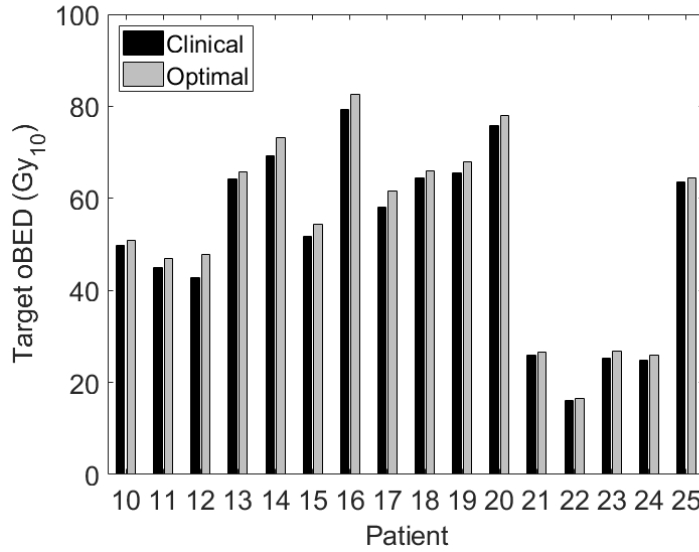
Figure 7 Target oBED values for the clinical and the optimal sequences for 16 patients with no OAR defined. The oBED values were calculated using the mono-exponential repair model and an α/β ratio of 10 Gy. Target oBED values for the clinical and the optimal sequences are shown in black and grey, respectively.

4.2 Therapeutic effect of using the optimal shot sequence and a reciprocal repair model

4.2.1 Patients with defined OARs

Figure 8 shows the therapeutic indices for the clinical and the optimal sequences for patients with defined OARs. These values are also including the relative change between them are summarized in **Table 11** (Appendix). The therapeutic indices for the optimal sequences were higher than for the clinical sequences in all patients. The relative change in the TI between both sequences varied from +0.4% to +4.9% (median +2.3%, mean +2.6% ± 1.7%). Patient 7 showed the lowest change (+0.4%) while patient 8 showed the highest change (+4.9%).
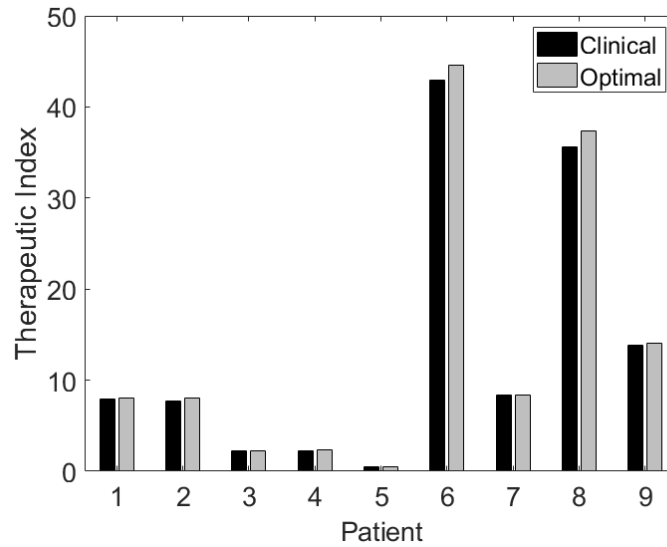
Figure 8 Therapeutic index values for the clinical shot sequence and the shot sequence with the highest therapeutic index (i.e. optimal shot sequence) for the nine patients with defined OARs. The oBED values used to calculate the therapeutic indices were calculated using the reciprocal repair model. The therapeutic indices for the clinical and the optimal sequences are shown in black and grey, respectively.

Figure 9 illustrates the oBED values for the target and the dose-limiting OAR for the clinical and optimal shot sequences for patients with defined OARs. These values are also presented in **Table 12** (Appendix). For the target, the mean relative change between the clinical and the optimal oBED values was +2.7% ± 1.7% (median 2.5%, range from +0.5% to +6.0%). The optimal target oBED values were higher than the clinical target oBED values for all patients. Additionally, the mean relative change between the clinical and the optimal oBED values for the dose-limiting OAR was 0.1% ± 1.2% (median 0.3%, range from -2.6 % to +1.6 %). The optimal OAR oBED values (i.e. oBED values for the dose-limiting OAR using the optimal shot sequence) were higher than the clinical OAR oBED values for all patients except for patient 4 (-0.4%) and patient 8 (-2.6%).
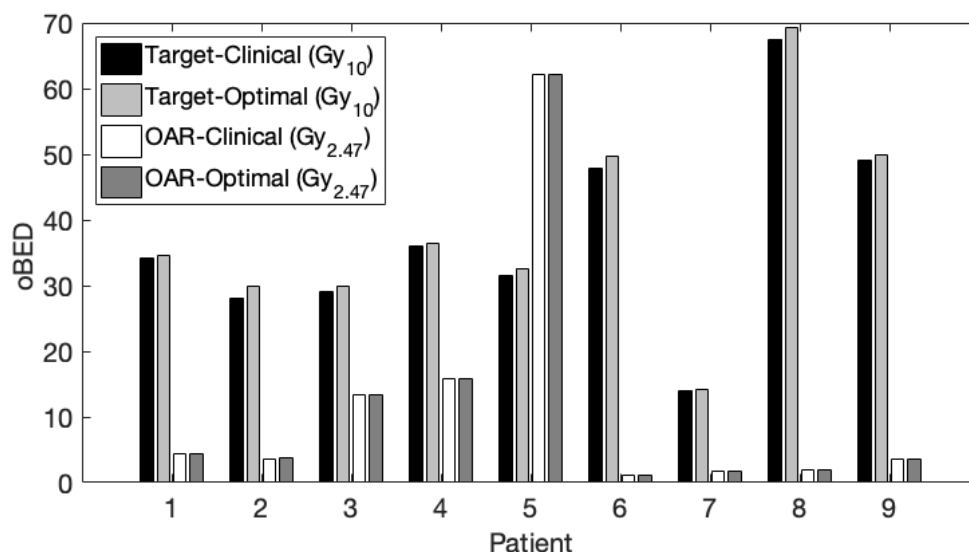
Figure 9 Clinical and optimal oBED values for the target and the dose-limiting OAR for the nine patients with defined OARs. The optimal sequence was defined as the shot sequence leading to the highest therapeutic index. The oBED values were calculated using the reciprocal repair model (α/β = 10 Gy for the target, and α/β = 2.47 Gy for the dose-limiting OAR). For the target, clinical and optimal oBED values are shown in black and light grey, respectively. For the dose-limiting OAR, clinical and optimal oBED values are shown in white and dark grey, respectively.

4.2.2 Patients with no defined OAR

Figure 10 shows the comparison of the target oBED values between the clinical and the optimal sequences for the patients without a defined OAR. The target oBED values for the clinical and the optimal sequences and the relative changes between them are presented in **Table 13** (Appendix). The target oBED values for the optimal sequences were higher than those for the clinical sequences for all the patients. The relative change between the target oBED values for the clinical and the optimal sequences varied within +1.0% and +8.4% (median +2.7%, mean +3.0% ± 1.8%). The lowest and highest changes were observed for patient 25 (+1.0%) and patient 12 (+8.4%), respectively.
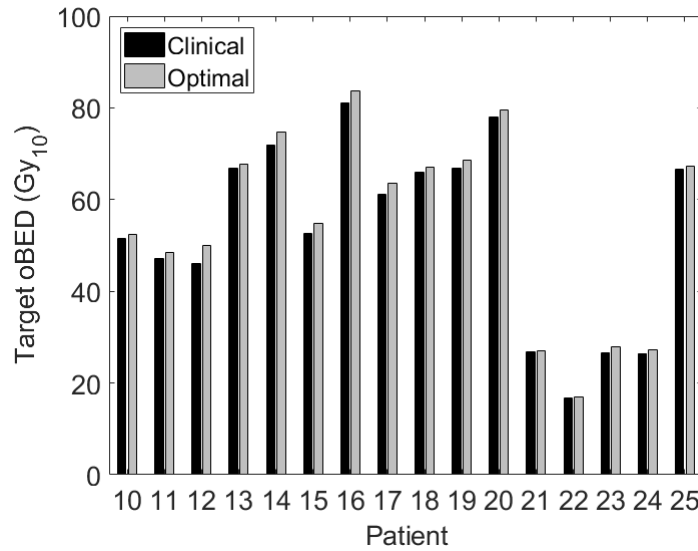
Figure 10 Target oBED values for the clinical and the optimal sequences for the 16 patients without a defined OAR. The oBED values were calculated using the reciprocal repair model and an α/β ratio of 10 Gy. Target oBED values for the clinical and the optimal sequences are shown in black and grey, respectively.

4.3 Therapeutic effect of using the optimal shot sequence and a bi-exponential repair model

4.3.1 Patients with defined OARs

The therapeutic indices for the clinical and the optimal sequences for the nine patients with defined OARs are presented in **Figure 11** as well as in **Table 14** (Appendix) which also includes the relative change between them. The TIs for the optimal sequences were higher than for the clinical sequences in all patients. The TI relative change between both sequences ranged from +0.7% to +7.7% (median +3.1%, mean +3.5% ± 2.7%). Patient 1 presented the lowest change (+0.7%) and patient 4 showed the highest change (+7.7%).
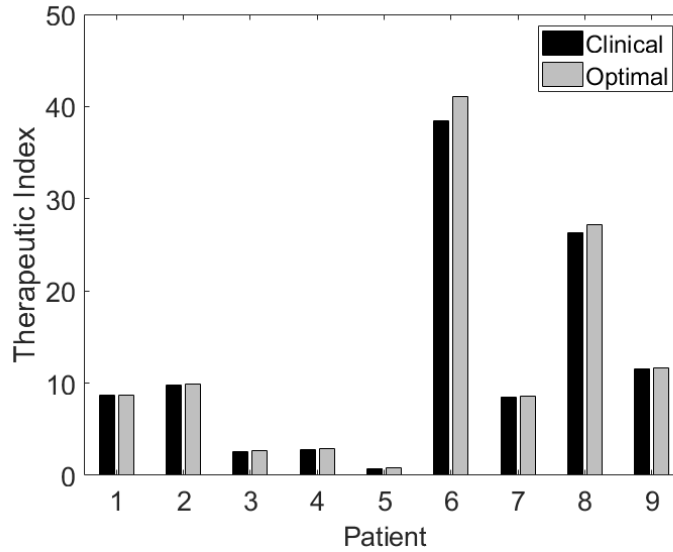
Figure 11 Therapeutic indices for the clinical and the optimal shot sequences (i.e. shot sequence with the highest therapeutic index) for the nine patients with defined OARs. The oBED values used to calculate the therapeutic indices were calculated using the bi-exponential repair model. The therapeutic indices for the clinical and the optimal sequences are shown in black and grey, respectively.

The oBED values for the target and the dose-limiting OAR for the clinical and optimal shot sequences for patients with defined OARs are illustrated in **Figure 12** and also presented in **Table 15** (Appendix). For the target, the mean relative change between the clinical and the optimal oBED values was +0.3% ± 1.6% (median +0.6%, range from -2.0% to +2.5 %). Four of nine patients showed optimal target oBED values lower than the clinical target oBED values. Moreover, for the dose-limiting OAR, the mean relative change between the clinical and the optimal oBED values was -3.0% ± 2.4% (median -3.1%, range from -8.0% to -0.3%). All nine patients showed optimal OAR oBED values lower than the clinical OAR oBED values.
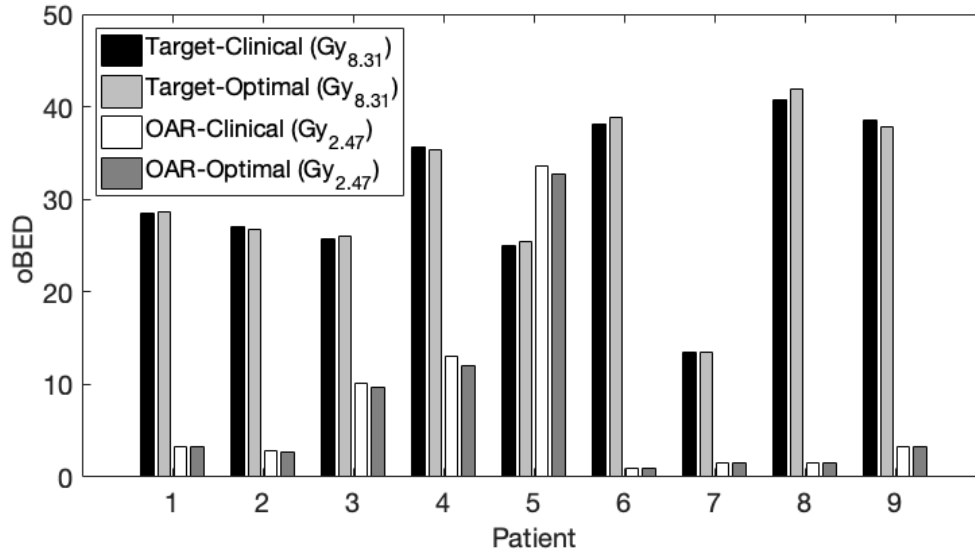
Figure 12 Clinical and optimal oBED values for the target and the dose-limiting OAR for the nine patients with defined OARs. The optimal sequence was defined as the shot sequence yielding the highest therapeutic index. The oBED values were calculated using the bi-exponential repair model (α/β = 8.31 Gy for the target, and α/β = 2.47 Gy for the dose-limiting OAR). For the target, clinical and optimal oBED values are shown in black and light grey, respectively. For the dose-limiting OAR, clinical and optimal oBED values are shown in white and dark grey, respectively.

4.3.2 Patients with no defined OAR

The target oBED values for the clinical and the optimal sequences for the 16 patients without a defined OAR can be observed in **Figure 13**. The target oBED values for the clinical sequences and the optimal sequences and the relative changes between them are shown in **Table 16** (Appendix). The target oBED values for the optimal sequences were higher than the target oBED values for the clinical sequences for all the patients. The relative change between the clinical and the optimal sequences ranged from +0.6% to +11.0% (median +2.5%, mean +2.9% ± 2.4%). The lowest and the highest changes were observed for patient 22 (+0.6%) and patient 12 (+11.0%), respectively.

Figure 13 Target oBED values for the clinical and the optimal sequences for the 16 patients with no OAR defined. The oBED values were calculated using the bi-exponential repair model and an α/β ratio of 8.31 Gy. Target oBED values for the clinical and the optimal sequences are shown in black and grey, respectively.

4.4 Therapeutic effect of using decayed Gamma Knife sources and a mono-exponential repair model

4.4.1 Patients with defined OARs

The TIs for the clinical and the optimal sequences for the nine patients with defined OARs are presented in **Figure 14**. These values, as well as the relative change between them, are presented in **Table 17** (Appendix). The TIs for the optimal sequences were higher than for the clinical sequences in all patients. The relative change in the TI between both sequences ranged from +0.6% to +11.8% (median +4.3%, mean +4.8% ± 3.4%). Patient 7 showed the lowest change (+0.6%), while patient 6 showed the highest change (+11.8%).
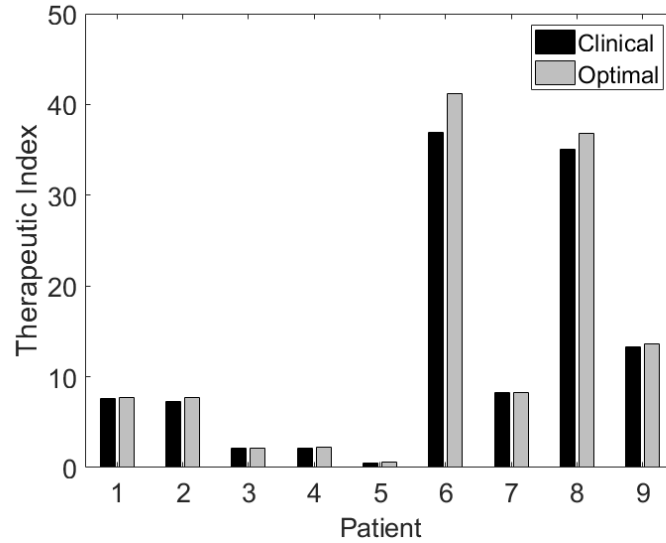
Figure 14 Therapeutic index (TI) values for the clinical and the optimal shot sequences (i.e. shot sequence with the highest TI) for the nine patients with defined OARs. The oBED values used to calculate the TIs were calculated using the mono-exponential repair model while considering the effect of source decay after one half-life. The TIs for the clinical and the optimal sequences are shown in black and grey, respectively.

Figure 15 shows the oBED values for the target and the dose-limiting OAR for the clinical and optimal shot sequences for the nine patients with defined OARs. These results are also presented in **Table 18** (Appendix). For the target, the mean relative change between the clinical and the optimal oBED values was +3.9% ± 3.2% (median +3.4%, range from +0.6% to +11.2%). Moreover, for the dose-limiting OAR, the mean relative change between the clinical and the optimal oBED values was -0.8% ± 3.2% (median -0.5%, range from -6.5% to +4.9%). For the target, patients 8 and patient 2 showed the lowest (+0.6%) and highest (+11.2%) oBED relative change, respectively. For the dose-limiting OAR, patients 6 and patient 2 showed the highest decrease (-6.5%) and highest increase (+4.9%) in oBED value, respectively.

Figure 15 Clinical and optimal oBED values for the target and the dose-limiting OAR for the nine patients with defined OARs. The optimal sequence was defined as the shot sequence producing the highest therapeutic index. The oBED values were calculated using the mono-exponential repair model (α/β = 10 Gy for the target, and α/β = 2.47 Gy for the dose-limiting OAR) while considering the effect of source decay after one half-life. The clinical and optimal target oBED values are shown in black and light grey, respectively. For the dose-limiting OAR, the clinical and optimal oBED values are shown in white and dark grey, respectively.

4.4.2 Patients with no defined OAR

Figure 16 illustrates the comparison of the target oBED values between the clinical and the optimal sequences for patients with no OAR defined. The target oBED values for the clinical sequences and the optimal sequences, as well as the relative changes between them, are presented in **Table 19** (Appendix). The target oBED values for the optimal sequences were higher than those for the clinical sequences for all the patients. The relative change between the clinical and the optimal sequences ranged from +1.8% to +10.1% (median +5.1%, mean +5.2% ± 2.4%). The lowest and highest changes were observed for patient 25 (+1.8%) and patient 12 (+10.1%), respectively.

Figure 16 Target oBED values for the clinical and the optimal sequences for the 16 patients without a defined OAR. The oBED values were calculated using the mono-exponential repair model and an α/β ratio of 10 Gy while considering the effect of source decay after one half-life. Target oBED values for the clinical and the optimal sequences are shown in black and grey, respectively.

4.5 Therapeutic effect of using decayed Gamma Knife sources and a reciprocal repair model

4.5.1 Patients with defined OARs

Figure 17 presents the TIs for the clinical and the optimal sequences for patients with defined OARs. These values together with the relative change between them are shown in **Table 20** (Appendix). The therapeutic indices for the optimal sequences were higher than for the clinical sequences in all patients. The TI relative change between both sequences varied from +0.5% to +7.3% (median +2.9%, mean +3.3% ± 2.1%). Patient 7 showed the lowest relative change (+0.5%), while patient 6 showed the highest relative change (+7.3%).
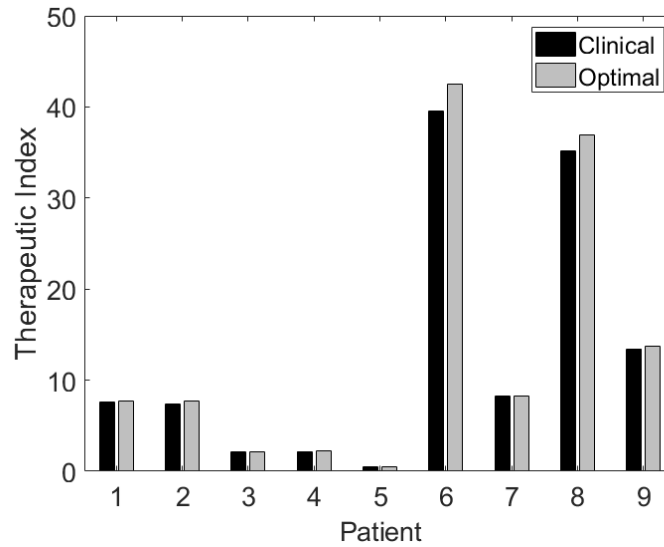
Figure 17 Therapeutic index (TI) values for the clinical and the optimal shot sequences (i.e. shot sequence with the highest TI) for the nine patients with defined OARs. The oBED values used to calculate the TIs were calculated using the reciprocal repair model while considering the effect of source decay after one half-life. The TIs for the clinical and the optimal sequences are shown in black and grey, respectively.

The oBED values for the target and the dose-limiting OAR for the clinical and optimal shot sequences for the nine patients with defined OARs are shown in **Figure 18** and also presented in **Table 21** (Appendix). For the target, the mean relative change between the clinical and the optimal oBED values was +3.2% ± 2.1% (median +2.2%, range from +0.7% to +7.6%). The optimal target oBED values were higher than the clinical target oBED values for all patients. In addition, for the dose-limiting OAR, the mean relative change between the clinical and the optimal oBED values was -0.2% ± 1.8% (median 0.2%, range from -3.3% to +2.8%). Six of the nine patients presented optimal OAR oBED values that were higher than the clinical OAR oBED values.
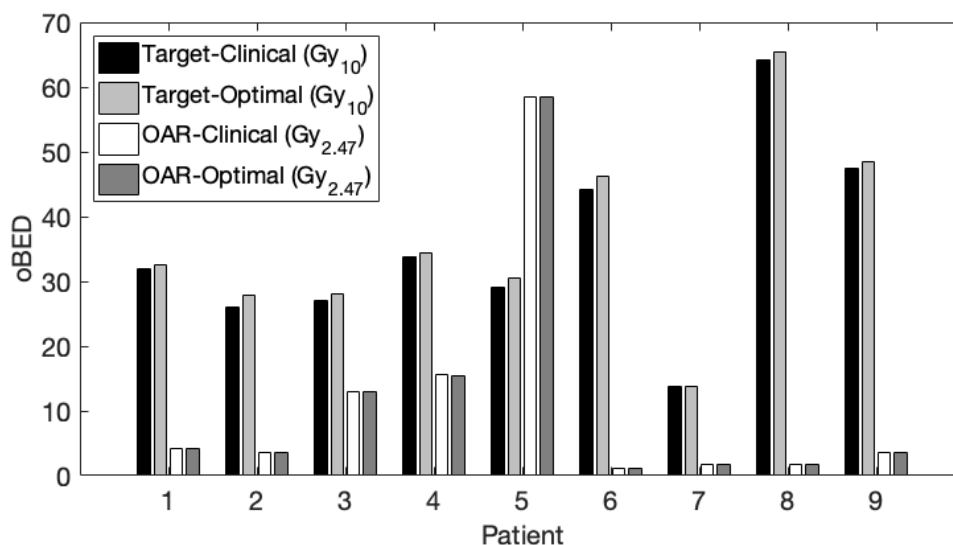
Figure 18 Clinical and optimal oBED values for the target and the dose-limiting OAR for the nine patients with defined OARs. The optimal sequence was defined as the shot sequence producing the highest TI. The oBED values were calculated using the reciprocal repair model (α/β = 10 Gy for the target, and α/β = 2.47 Gy for the dose-limiting OAR) model while considering the effect of source decay after one half-life. For the target, clinical and optimal oBED values are shown in black and light grey, respectively. For the dose-limiting OAR, clinical and optimal oBED values are shown in white and dark grey, respectively.

4.5.2 Patients with no defined OAR

Figure 19 shows the comparison of the target oBED values between the clinical and the optimal sequences for the 16 patients without a defined OAR. The target oBED values for the clinical sequences and the optimal sequences together with the relative changes between them are summarized in **Table 22** (Appendix). The target oBED values for the optimal sequences were higher than those for the clinical sequences for all the patients. The relative change between the clinical and the optimal sequences varied between +1.1% and +8.4% (median +3.3%, mean +3.5% ± 1.9%). The lowest and highest changes were observed for patient 25 (+1.1%) and patient 12 (+8.4%), respectively.
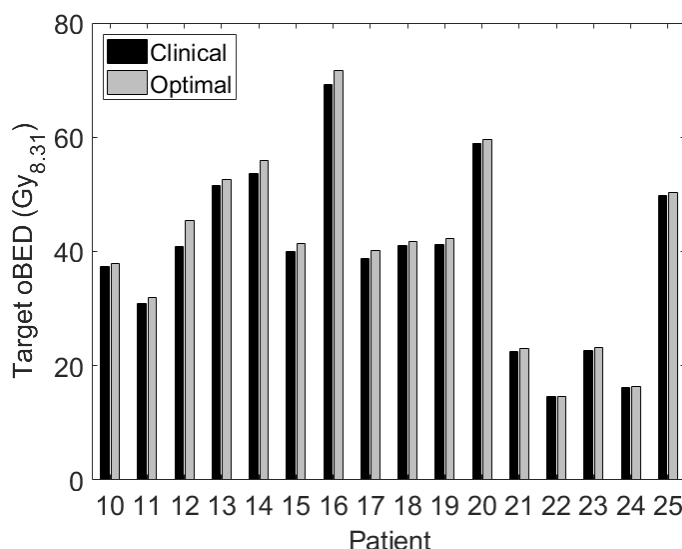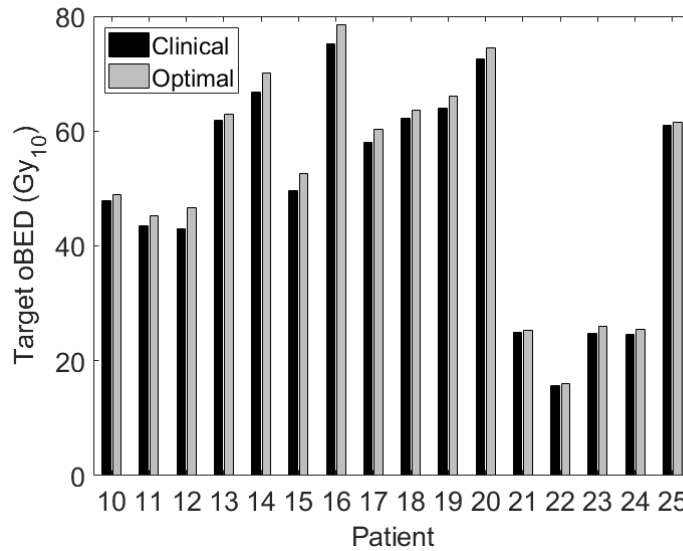
Figure 19 Target oBED values for the clinical and the optimal sequences for the 16 patients with no OAR defined. The oBED values were calculated using the reciprocal repair model and an α/β ratio of 10 Gy while considering the effect of source decay after one half-life. Target oBED values for the clinical and the optimal sequences are shown in black and grey, respectively.

4.6 Therapeutic effect of using decayed Gamma Knife sources and a bi-exponential repair model

4.6.1 Patients with OAR defined

The TIs for the clinical and the optimal sequences for the nine patients with defined OARs are shown in **Figure 20**. These values, as well as the relative change between them, are presented in **Table 23** (Appendix). The TIs for the optimal sequences were higher than for the clinical sequences in all patients. The TI relative change between both sequences ranged from +0.1% to +5.8% (median +2.9%, mean +2.8% ± 2.0%). Patient 9 showed the lowest change (+0.1%), while patient 4 showed the highest change (+5.8%).
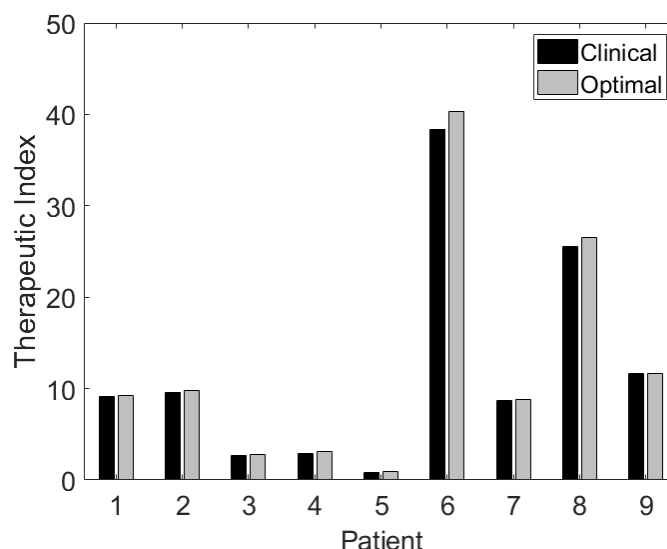
Figure 20 Therapeutic index (TI) values for the clinical and the optimal shot sequences (i.e. shot sequence with the highest TI) for the nine patients with defined OAR. The oBED values used to calculate the therapeutic indices were calculated using the bi-exponential repair model while considering the effect of source decay after one half-life. The TIs for the clinical and the optimal sequences are shown in black and grey, respectively.

The oBED values for the target and the dose-limiting OAR for the clinical and optimal shot sequences for the nine patients with defined OARs are illustrated in **Figure 21** and also presented in **Table 24** (Appendix). For the target, the mean relative change between the clinical and the optimal oBED values was +1.2% ± 1.6% (median +1.1%, range from -1.5% to +4.2%). For patient 4 (-1.5%) and patient 7 (-0.4%), the optimal oBED value was lower than the clinical oBED value. For the dose-limiting OAR, the mean relative change between the clinical and the optimal oBED values was -1.5% ± 2.5% (median -1.2%, range from -7.0% to +1.2%). Patient 1 (+0.1%), patient 8 (+0.7%), and patient 9 (+1.2%) showed higher optimal oBED values than the clinical oBED values.
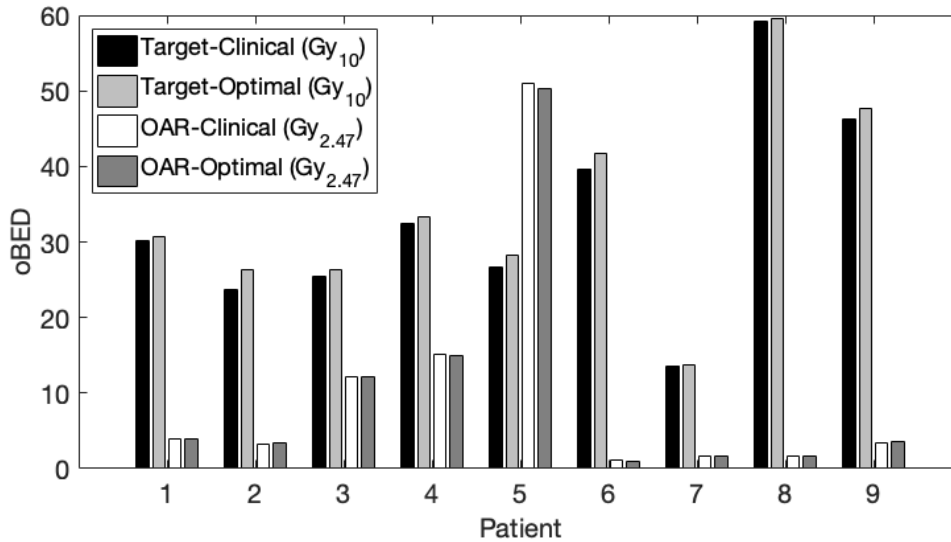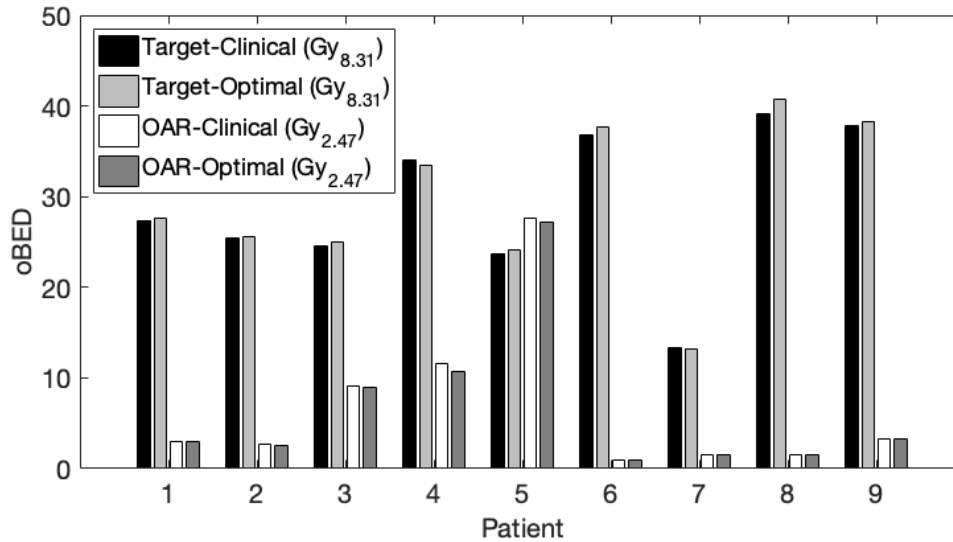
Figure 21 Clinical and optimal oBED values for the target and the dose-limiting OAR for the nine patients with defined OAR. The optimal sequence was defined as the shot sequence producing the highest TI. The oBED values were calculated using the bi-exponential repair model (α/β = 8.31 Gy for the target, and α/β = 2.47 Gy for the dose-limiting OAR) while considering the effect of source decay after one half-life. For the target, clinical and optimal oBED values are shown in black and light grey, respectively. For the dose-limiting OAR, clinical and optimal oBED values are shown in white and dark grey, respectively.

4.6.2 Patients with no defined OAR

Figure 22 illustrates the comparison of the target oBED values between the clinical and the optimal sequences for the 16 patients with no OAR defined. The target oBED values for the clinical and optimal sequences, as well as the relative changes between them, are presented in **Table 25** (Appendix). The target oBED values for the optimal sequences were higher than those for the clinical sequences for all patients. The relative change between the clinical and the optimal sequences ranged from +0.9% to +9.1% (median +2.7%, mean +3.4% ± 2.1%). The lowest and highest changes were observed for patient 22 (+0.9%) and patient 12 (+9.1%), respectively.
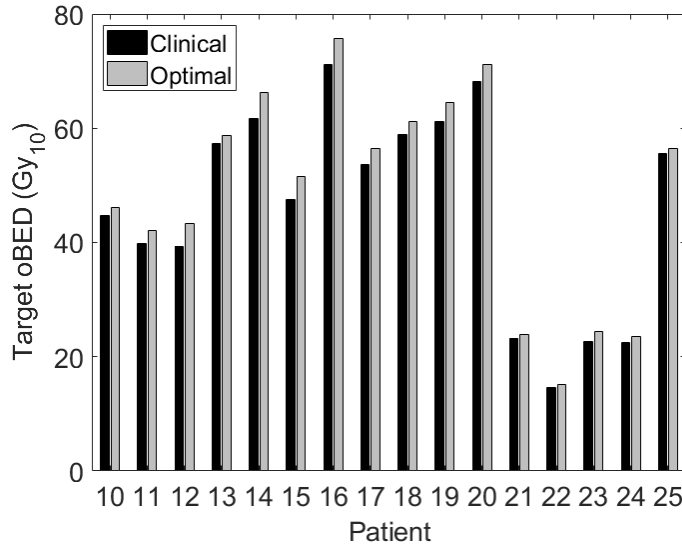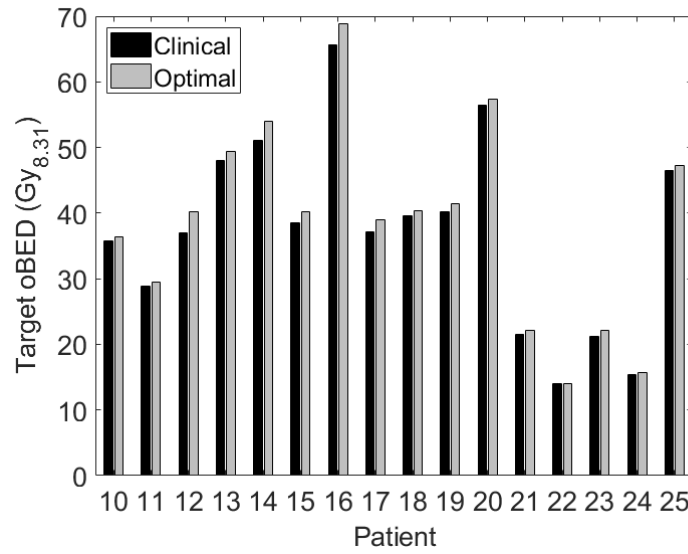
Figure 22 Target oBED values for the clinical and the optimal sequences for the 16 patients with no OAR defined. The oBED values were calculated using the bi-exponential repair model and an α/β ratio of 8.31 Gy while considering the effect of source decay after one half-life. Target oBED values for the clinical and the optimal sequences are shown in black and grey, respectively.

5 DISCUSSION

The present study evaluated the impact of changing the shot sequence for the same absorbed dose distribution on the radiobiological response for 25 patients with malignant and benign brain tumors treated with Gamma Knife radiosurgery. The patients were categorized into two groups: patients with defined OARs and patients with no OAR defined. Because of the inhomogeneous dose distribution in GK radiosurgery, the overall biologically effective dose (oBED) [91] was used to represent the radiobiological effect both in the targets and in the OARs. The oBED values for the targets and the OARs were calculated with three different repair models [89] (mono-exponential, reciprocal and bi-exponential). The shot sequence was the only parameter changed compared to the clinical plans. Additionally, the effect of the physical decay of the GK sources on the biological effectiveness of the treatments was evaluated by simulating plans with GK sources decayed after one half-life (5.26 years for ^{60}Co).

The results of this study showed that there is an optimal shot sequence, which differs from the clinical shot sequence (**Table 26**, Appendix) and which allows improvement in the biological effect in GK radiosurgery. The improvement in the treatment biological effectiveness can be defined as a higher therapeutic index or as a higher target oBED. A higher therapeutic index allows higher target oBED values for the same OAR oBED or lower OAR oBED values for the same target oBED. How to optimize a plan using biologically effective doses (such as the oBED) depends on the case-by-case analysis by the treating physician.

Table 6 shows the improvement in the biological effect achieved by applying an optimal shot sequence, when compared to the clinical shot sequence, for multiple repair models both when using GK sources with the clinical activity (non-decayed) and when GK sources decayed after one half-life (decayed) were considered.

As observed in **Table 6**, when using non-decayed GK sources, the mean improvement in the biological effect (considering both improvement in the therapeutic indices and in the target oBED values) was 4.3% ± 2.7% (median 3.8%, range from 0.2% to 12.1%), 2.9 ± 1.7% (median 2.7%, range from 0.4% to 8.4%) and 3.1% ± 2.4% (median 2.6%, range from 0.6% to 11.0%) for the mono-exponential, reciprocal and bi-exponential repair models, respectively. When using decayed GK sources, the mean improvement in the biological effect was 5.0% ± 2.7% (median 5.0%, range from 0.6% to 11.8%), 3.4% ± 1.9% (median 3.2%, range from 0.5% to 8.4%) and 3.2% ± 2.0% (median 2.9%, range from 0.1% to 9.1%) for the mono-exponential, reciprocal and bi-exponential repair models, respectively. Patient 12 (meningioma, target of 0.27 cc, 16 Gy prescribed at the 50% isodose line, 7 shots, no OAR defined) showed the highest treatment improvement overall. However, this patient does not show any extreme parameter for dose, target volume or number of shots, which indicates that a combination of multiple factors (including the shape of the target and its proximity to

the OARs) needs to be individually analyzed to determine the potential improvement in the treatment radiobiological effect.

Table 6 Improvement in the treatment radiobiological effectiveness by using an optimal shot sequence compared to the clinical shot sequence. The improvement in the biological effect was measured using three repair models: mono-exponential, reciprocal and bi-exponential. The analysis was performed for GK sources with the same activity as in the clinical plan (i.e. non-decayed) and for simulated GK sources decayed after one half-life (i.e. decayed). Values are given as the relative change (%) in the therapeutic index or in the target oBED between the optimal and the clinical shot sequences.

| Patient ID | Repair model | | | | | |
| | Mono-exponential | | Reciprocal | | Bi-exponential | |
	Non-decayed	Decayed	Non-decayed	Decayed	Non-decayed	Decayed
[*]Pt 1	+1.3	+2.0	+1.1	+1.4	+0.7	+0.8
[*]Pt 2	+5.5	+5.9	+4.5	+4.7	+2.1	+1.4
[*]Pt 3	+3.2	+4.3	+2.3	+2.9	+4.3	+2.9
[*]Pt 4	+2.2	+3.7	+1.3	+2.3	+7.7	+5.8
[*]Pt 5	+5.8	+7.7	+3.9	+4.0	+5.4	+3.5
[*]Pt 6	+10.0	+11.8	+3.8	+7.3	+6.9	+5.1
[*]Pt 7	+0.2	+0.6	+0.4	+0.5	+1.1	+1.4
[*]Pt 8	+7.7	+5.0	+4.9	+5.0	+3.1	+3.9
[*]Pt 9	+1.9	+2.5	+1.5	+1.8	+0.8	+0.1
[$]Pt 10	+2.3	+3.2	+1.7	+2.1	+1.4	+1.8
[$]Pt 11	+4.8	+5.9	+3.1	+3.7	+3.2	+2.5
[$]Pt 12	+12.1	+10.1	+8.4	+8.4	+11.0	+9.1
[$]Pt 13	+2.4	+2.3	+1.6	+1.6	+2.1	+2.9
[$]Pt 14	+5.7	+7.4	+4.0	+4.9	+4.2	+5.7
[$]Pt 15	+5.3	+8.6	+4.1	+5.8	+3.1	+4.3
[$]Pt 16	+4.1	+6.3	+3.1	+4.3	+3.5	+4.8
[$]Pt 17	+6.2	+5.5	+4.0	+4.1	+3.8	+5.0
[$]Pt 18	+2.6	+3.6	+1.8	+2.2	+1.7	+2.3
[$]Pt 19	+3.8	+5.2	+2.7	+3.3	+2.4	+3.2
[$]Pt 20	+2.9	+4.4	+2.1	+2.8	+1.1	+1.5
[$]Pt 21	+2.2	+2.5	+1.1	+1.7	+2.6	+2.5
[$]Pt 22	+2.4	+3.2	+1.7	+2.1	+0.6	+0.9
[$]Pt 23	+6.3	+7.2	+4.3	+4.9	+2.8	+3.9
[$]Pt 24	+4.5	+5.0	+2.8	+3.2	+1.5	+1.9
[$]Pt 25	+1.6	+1.8	+1.0	+1.1	+1.1	+1.5

[*] Improvement calculated as the relative change in the therapeutic index
[$] Improvement calculated as the relative change in the target oBED

The mean improvement calculated with the therapeutic index (nine patients) was smaller than the mean improvement calculated with the target oBED (16 patients) for all the simulated scenarios, except when using a bi-exponential repair model with non-

decayed GK sources. This can be generally explained by the fact that the target oBED optimization does not consider the restriction imposed by the oBED in the OARs. Thus, optimization considering the therapeutic index may produce better treatment characteristics than simply optimizing the target biological effect. Furthermore, the mean improvement achieved for the decayed GK sources was larger than the mean improvement for the non-decayed sources for all the evaluated repair models. This demonstrates that in longer GK treatments (with lower dose rates) there is a higher probability of biological repair, and therefore, the effect of biologically-based optimization is higher. Additionally, it could have been expected that plans with more shots would allow bigger improvements in the biological effect of the treatment, as many more shot combinations can be achieved. However, there was no correlation between the number of shots and the percentage of improvement as other factors such as the prescribed dose, the prescription isodose line and the heterogeneity of the dose distribution are also of high relevance to define the achievable improvement in the biological effect.

The improvement results obtained in this thesis are in line with previous studies [7,18]. Ma et al. showed a variation in the single equivalent uniform dose (sEUD) (another dose representation of the radiobiological effect) of less than 4% between the clinical sequences and sequences that produced maximum sEUD values for the target [7]. Additionally, Andisheh et al. showed that the brain BED was reduced between 2% and 8% in GK radiosurgery when applying a more complex algorithm to optimize the therapeutic index [18]. The algorithm applied by Andisheh et al. used a bi-exponential repair model and included variation not only of the shot sequence but also of the dose rates and the dose fractions, while conserving the total absorbed dose for the target [18]. In this thesis, the reduction in the OAR oBED for the optimal shot sequences determined by the highest therapeutic index using a bi-exponential repair model varied from 0.3% to 8.0% (median 3.1%, mean 3.0% ± 2.2%).

Table 7 shows the relative change in the treatment effectiveness for the clinical plan when decayed GK sources are used (decayed after one half-life). Treatment effectiveness was calculated with the therapeutic index (nine patients) or with the target oBED (16 patients).

In **Table 7,** the change in the effectiveness for the clinical plan with decayed GK sources differs significantly when calculated with the therapeutic index or with the target oBED. Therefore, separate analyses need to be carried out. When using decayed GK sources, the therapeutic index (nine patients) decreased 5.4% ± 5.1% (median 5.0%, range from decrease of 17.6% to increase of 1.1%), decreased 3.7% ± 1.9% (median 4.2%, range from 1.4% to 7.9%) and increased 3.8% ± 5.6% (median 2.3%, range from decrease of 3.1% to increase of 16.2%) for the mono-exponential, reciprocal and bi-exponential repair models, respectively. For the mono-exponential and the reciprocal repair models, it was observed a higher increase in the repair of sublethal damage in the target than in the dose-limiting OAR (except for patient 8, mono-exponential model), leading to a general decrease in the therapeutic indices for

clinical plans with decayed GK sources. For patient 8, the increase in the therapeutic index when using decayed sources for the mono-exponential model could be produced by a low probability of repair in the target because of the high prescribed dose (25 Gy, highest dose among all the 25 patients) while repair was still possible in the dose-limiting OAR, which received a much lower dose (less than $2\ Gy_{2.47}$). On the other hand, it can be observed how the bi-exponential model favors repair in structures with lower doses (such as the OARs) compared to structures receiving high doses (such as the targets) for lower dose rates (obtained with decayed GK sources). This led to the general increase in the therapeutic indices observed for the bi-exponential model with decayed sources (except for patients 2 and 8).

Table 7 Relative change in the treatment effectiveness for the clinical plan when the activity of the sources is decayed after one half-life. Values are given as the relative change (%) in the therapeutic index or in the target oBED.

Patient ID	Repair models		
	Mono-exponential	Reciprocal	Bi-exponential
*Pt 1	-4.8	-4.2	5.8
*Pt 2	-5.0	-4.4	-1.3
*Pt 3	-5.0	-4.6	6.7
*Pt 4	-5.3	-4.4	7.3
*Pt 5	0.0	-2.0	16.2
*Pt 6	-8.0	-7.9	0.0
*Pt 7	-17.6	-1.7	2.3
*Pt 8	1.1	-1.4	-3.1
*Pt 9	-3.7	-2.9	0.5
$Pt 10	-10.4	-7.0	-4.4
$Pt 11	-11.5	-7.5	-6.7
$Pt 12	-7.8	-6.7	-9.7
$Pt 13	-10.7	-7.4	-6.9
$Pt 14	-10.8	-7.1	-4.9
$Pt 15	-8.2	-5.6	-3.8
$Pt 16	-10.3	-7.2	-5.1
$Pt 17	-7.6	-5.1	-4.1
$Pt 18	-8.4	-5.5	-3.8
$Pt 19	-6.5	-4.3	-2.8
$Pt 20	-10.2	-6.9	-4.2
$Pt 21	-10.3	-7.2	-3.8
$Pt 22	-9.1	-6.4	-4.4
$Pt 23	-10.1	-7.2	-5.8
$Pt 24	-9.7	-6.9	-4.5
$Pt 25	-12.6	-8.5	-6.6

* Improvement calculated as the relative difference in the therapeutic index
$ Improvement calculated as the relative difference in the target oBED

For patients with no defined OAR, the target oBED decreased for all the patients and repair models when using GK sources decayed after one half-life (**Table 7**). Thus,

decreases in the target oBED of 9.6% ± 1.5% (median 10.15%, range from 6.5% to 12.6%), 6.7% ± 1.0% (median 7.0%, range from 4.3% to 8.5%) and of 5.1% ± 1.6% (median 4.5%, range from 2.8% to 9.7%) were observed when using decayed sources for the mono-exponential, reciprocal and bi-exponential repair models, respectively. Lower target oBED values were expected for decayed GK sources as lower dose rates increase the probability of sublethal repair, thus producing a lower radiobiological effect (and lower oBED values). However, the clinical impact of lower dose rates in GK radiosurgery seems to be moderate, as no significant changes in the clinical treatment outcome have been found [98,99] while an increase in disease-related symptoms [98] but also a decrease in side effects (produced by radiation-induced damage to the OARs) [99] have been reported for lower dose rates. Nevertheless, the effect of different dose rates in GK radiosurgery is difficult to assess in clinical practice, as patients usually receive adjuvant systemic treatment (e.g. chemotherapy), which influences the biological response to the GK radiosurgery treatment [99]. Hence, the clinical evaluation of radiation-induced toxicities becomes highly complex [99].

The decrease in the target oBED values obtained in this thesis is in line with previous studies which also analyzed the effect of decayed GK sources after one half-life [100], Howell et al. showed a reduction in the target BED of approximately 11% for GK sources after one half-life decay (GK Perfexion®, 1 patient, prescribed dose of 13.03 Gy, 12 shots, 26 min clinical plan) [100]. The GK Perfexion® used by Hopewell et al. has a similar treatment delivery technique as the GK Icon™ (used in this study), which allows a fair comparison. The use of a different Gamma Knife model (such as models B or C) would significantly affect the BED values because of the much longer treatment times.

Overall, oBED values calculated with the mono-exponential and the reciprocal repair models were similar among them while oBED values calculated with the bi-exponential model were considerably smaller than values obtained with the other two repair models (**Table 8**, **Table 9**, **Table 11**, **Table 12**, **Table 14**, and **Table 15**). Additionally, in 23 out of 25 patients (except for patients 2 and 7), the optimal sequence calculated with the mono-exponential model was equal to the optimal sequence obtained with the reciprocal model (**Table 26**, Appendix). On the other hand, the optimal shot sequence attained with the bi-exponential model was different to the optimal sequence obtained with the mono-exponential and the reciprocal models for all patients, except for patients 17, 20, 21, and 24 for whom the optimal sequence was the same with the three evaluated repair models. The use of a model with two different repair half-lives (fast and slow repair components) and different radiobiological parameters (especially a smaller α/β ratio) may have produced smaller oBED values for the bi-exponential model. In addition, the effect of the variations in the dose rate over time produced by the change of the shot sequence differed for the bi-exponential model, compared to the mono-exponential and the reciprocal models. However, Hopewell et al. [100] stated that the bi-exponential is the best repair model to describe sublethal damage (especially for healthy brain tissue) as repair models that do not consider a fast repair component (such as the mono-exponential model) could considerably underestimate

the importance of the short time between shots in GK radiosurgery, which is approximately of 0.1 min for the Gamma Knife® Icon™. For the reciprocal model, the use of a variable effective half-life (varying with time) may compensate for the lack of a fast repair component and, therefore, may produce more accurate results than the mono-exponential model, as shown by Fowler [93]. Additionally, it is important to consider the beam-off times (zero dose rate) between each shot for the oBED calculations (as done in this thesis), as considerable fast repair may occur during these periods. Moreover, it is essential to include any time gaps or interruptions (e.g. due to patient movement or discomfort) that may happen during the treatment, as shown by Putora et al. [101]. For fractionated GK radiosurgery, the time between fractions is also of great importance to determine the total biological effect as total repair can be achieved between 15 h and 24 h for most tissues [100].

Additional limitations in the oBED calculations in this thesis are the large uncertainty in the model parameters for the three evaluated repair models (as some parameters are derived from animal studies) [100] as well as the fact that the same parameters were used for all targets and all OARs, without distinguishing for tumor type or for different OARs. The use of specific radiobiological parameters for each type or tumor and OAR would produce more clinically relevant results. However, accurate radiobiological parameters for multiple brain structures and types of brain tumors cannot be found in the literature. Moreover, in patients with more than 10 shots (five patients), only 1,000 random shot combinations were evaluated to determine the best shot sequence, which could have produced sub-optimal shot sequences for these patients.

In spite of the differences in the evaluated repair models and the described limitations in the study, the improvement in the biological effect achieved with the three evaluated repair models was similar for the three evaluated repair models.

6 CONCLUSION

The analyses conducted in this thesis showed that the time pattern of the dose deposition is an important determinant of the radiobiological effect in GK radiosurgery, both for the target and for the organs at risk. Thus, after exploring all possible shot combinations for the same dose distribution, an optimal shot sequence yielding maximum radiobiological effectiveness can be determined in GK radiosurgery. The optimization of the GK treatment can be defined by the sequence resulting in the highest target oBED or by the sequence with the highest therapeutic index. The latter is expected to produce better overall treatment characteristics. However, how to optimize the GK treatment based on the radiobiological effectiveness is a case-by-case medical decision. Moreover, the physical decay of the GK sources after one half-life showed a considerable decrease in the radiobiological effectiveness in the target for the same dose distribution.

The three sublethal repair models analyzed in this thesis produced different oBED values for the target and the OARs, with the mono-exponential and the reciprocal models producing similar results and the bi-exponential model delivering smaller oBED values. In addition, the optimal shot sequences obtained with the mono-exponential and the reciprocal models were the same for most patients, while the optimal shot sequences attained with the bi-exponential model differed from the optimal sequences determined by the other evaluated repair models for most patients. However, the relative change in the target oBED between the optimal and the clinical sequences was comparable for all the three repair models. This same tendency was observed in the analysis of decayed GK sources on the radiobiological effect in GK radiosurgery.

7 REFERENCES

1. Hatiboglu, M. A. & Sawaya, R. Intracranial Stereotactic Radiosurgery. *Neuro. Oncol.* **12**, 1083–1084 (2010).
2. Amichetti, M., Amelio, D. & Minniti, G. Radiosurgery with photons or protons for benign and malignant tumours of the skull base: a review. *Radiat. Oncol.* **7**, 210 (2012).
3. Kondziolka, D., Shin, S. M., Brunswick, A., Kim, I. & Silverman, J. S. The biology of radiosurgery and its clinical applications for brain tumors. *Neuro. Oncol.* **17**, 29–44 (2014).
4. Stieler, F. *et al.* Adaptive fractionated stereotactic Gamma Knife radiotherapy of meningioma using integrated stereotactic cone-beam-CT and adaptive re-planning (a-gkFSRT). *Strahlentherapie und Onkol.* **192**, 815–819 (2016).
5. Frischer, J. M. *et al.* Evaluation of dose-staged Gamma Knife radiosurgical treatment method for high-risk brain metastases. *World Neurosurg.* **94**, 352–359 (2016).
6. Balagamwala. Principles of Radiobiology of Stereotactic Radiosurgery and Clinical Applications in the Central Nervous System. *Technol. Cancer Res. Treat.* **11**, (2012).
7. Ma, L. *et al.* Shot sequencing based on biological equivalent dose considerations for multiple isocenter Gamma Knife radiosurgery. *Phys. Med. Biol.* **56**, 7247 (2011).
8. Flickinger, J. C., Dade^Lunsford, L., Wu, A., Maitz, A. H. & Kalend, A. M. Treatment planning for gamma knife radiosurgery with multiple isocenters. *Int. J. Radiat. Oncol. Biol. Phys.* **18**, 1495–1501 (1990).
9. Wu, Q. J. *et al.* Real-time inverse planning for Gamma Knife radiosurgery. *Med. Phys.* **30**, 2988–2995 (2003).
10. Arai, Y. *et al.* Does the Gamma Knife dose rate affect outcomes in radiosurgery for trigeminal neuralgia? *J. Neurosurg.* **113**, 168–171 (2010).
11. Lee, J. Y. K. *et al.* Higher dose rate Gamma Knife radiosurgery may provide earlier and longer-lasting pain relief for patients with trigeminal neuralgia. *J. Neurosurg.* **123**, 961–968 (2015).
12. Grudzinski, J. J., Tomé, W., Weichert, J. P. & Jeraj, R. The biological effectiveness of targeted radionuclide therapy based on a whole-body pharmacokinetic model. *Phys. Med. Biol.* **55**, 5723 (2010).
13. Brenner, D. J. The Linear-Quadratic Model Is an Appropriate Methodology for Determining Isoeffective Doses at Large Doses Per Fraction. *Semin. Radiat. Oncol.* **18**, 234–239 (2008).
14. Mason, A. J. *et al.* Interaction between the biological effects of high- and low-LET radiation dose components in a mixed field exposure. *Int. J. Radiat. Biol.* **87**, 1162–1172 (2011).
15. Hopewell, J. W. *et al.* Application of the concept of biologically effective dose (BED) to patients with Vestibular Schwannomas treated by radiosurgery. *J. radiosurgery SBRT* **2**, 257 (2013).
16. Hallgren, S. *et al.* Effects of variations in overall treatment time on the clonogenic survival of V79-4 cells: Implications for radiosurgery. *J. radiosurgery SBRT* **6**, 1 (2019).
17. Murphy, M. J. *et al.* Patterns of patient movement during frameless image-guided radiosurgery. *Int J Radiat Oncol Biol Phys* **55**, (2003).
18. Andisheh, B., Belkić, D., Mavroidis, P., Alahverdi, M. & Lind, B. K. Improving the

therapeutic ratio in stereotactic radiosurgery: optimizing treatment protocols based on kinetics of repair of sublethal radiation damage. *Technol. Cancer Res. Treat.* **12**, 349–361 (2013).

19. Paganetti, H. Changes in tumor cell response due to prolonged dose delivery times in fractionated radiation therapy. *Int. J. Radiat. Oncol. Biol. Phys.* **63**, 892–900 (2005).

20. Steel, G. G. *et al.* The dose-rate effect in human tumour cells. *Radiother. Oncol.* **9**, 299–310 (1987).

21. Nakamura, J. L. *et al.* Dose conformity of gamma knife radiosurgery and risk factors for complications. *Int. J. Radiat. Oncol. Biol. Phys.* **51**, 1313–1319 (2001).

22. Leksell Gamma Knife® Icon™ from Elekta. Available at: https://careforthebrain.com/. (Accessed: 24th February 2020)

23. AlDahlawi, I., Prasad, D. & Podgorsak, M. B. Evaluation of stability of stereotactic space defined by cone-beam CT for the Leksell Gamma Knife Icon. *J. Appl. Clin. Med. Phys.* **18**, 67–72 (2017).

24. Chin, L. S. & Regine, W. F. *Principles and practice of stereotactic radiosurgery*. (Springer Science & Business Media, 2010).

25. Porter, N. C. *Principles and Practice of Stereotactic Radiosurgery*. *Trigeminal Neuralgia: Medical Management Perspective* (2008). doi:10.1017/CBO9781107415324.004

26. Zeverino, M. *et al.* Commissioning of the Leksell Gamma Knife® Icon™: *Med. Phys.* **44**, 355–363 (2017).

27. Baumert, B. G., Egli, P., Studer, S., Dehing, C. & Davis, J. B. Repositioning accuracy of fractionated stereotactic irradiation: assessment of isocentre alignment for different dental fixations by using sequential CT scanning. *Radiother. Oncol.* **74**, 61–66 (2005).

28. Bednarz, G. *et al.* Report on a randomized trial comparing two forms of immobilization of the head for fractionated stereotactic radiotherapy. *Med. Phys.* **36**, 12–17 (2009).

29. Boda-Heggemann, J. *et al.* Repositioning accuracy of two different mask systems—3D revisited: comparison using true 3D/3D matching with cone-beam CT. *Int. J. Radiat. Oncol. Biol. Phys.* **66**, 1568–1575 (2006).

30. Masi, L. *et al.* Cone beam CT image guidance for intracranial stereotactic treatments: comparison with a frame guided set-up. *Int. J. Radiat. Oncol. Biol. Phys.* **71**, 926–933 (2008).

31. Chung, C. *et al.* Clinical Evaluation of a Novel Thermoplastic Mask System With Intrafraction Motion Monitoring Using IR Tracking and Cone Beam CT for Gamma Knife Radiosurgery. *Int. J. Radiat. Oncol. • Biol. • Phys.* **90**, S848 (2014).

32. Leksell GammaPlan® 11. Available at: https://www.elekta.com/radiosurgery/leksell-gammaplan/leksell-gammaplan-11/. (Accessed: 24th February 2020)

33. Sjölund, J., Riad, S., Hennix, M. & Nordström, H. A linear programming approach to inverse planning in Gamma Knife radiosurgery. *Med. Phys.* **46**, 1533–1544 (2019).

34. Rojas-Villabona, A., Kitchen, N. & Paddick, I. Investigation of dosimetric differences between the TMR 10 and convolution algorithm for Gamma Knife stereotactic radiosurgery. *J. Appl. Clin. Med. Phys.* **17**, 217–229 (2016).

35. Xu, A. *et al.* Dose differences between the three dose calculation algorithms in Leksell GammaPlan. *J. Appl. Clin. Med. Phys.* **15**, 89–99 (2014).

36. Pipek, J., Novotný Jr, J., Novotný, J. & Kozubíková, P. Comparison of dose calculation algorithms for Leksell Gamma Knife Perfexion using Monte Carlo

voxel phantoms. *Lékař a Tech. Technol.* **45**, 75–81 (2015).

37. Wright, G., Hatfield, P., Loughrey, C., Reiner, B. & Bownes, P. A method for scoring treatment time efficiency of Gamma Knife radiosurgical treatment plans for brain metastases. *Med. Phys.* **40**, 021723 (2013).

38. Sandström, H., Jokura, H., Chung, C. & Toma-Dasu, I. Multi-institutional study of the variability in target delineation for six targets commonly treated with radiosurgery. *Acta Oncol. (Madr).* **57**, 1515–1520 (2018).

39. Burnet, N. G., Thomas, S. J., Burton, K. E. & Jefferies, S. J. Defining the tumour and target volumes for radiotherapy. *Cancer Imaging* **4**, 153 (2004).

40. Millar, W. T. *et al.* The role of the concept of biologically effective dose (BED) in treatment planning in radiosurgery. *Phys. Medica* **31**, 627–633 (2015).

41. Prasad, S., Podgorsak, M., Plunkett, R. & Prasad, D. An evaluation of the ICON® mask fixation: curing characteristics of the thermoplastic fixation and implications for patient workflow. *Radiol. Oncol.* **52**, 229–232 (2018).

42. Stieler, F. *et al.* Validation of frame-based positioning accuracy with cone-beam computed tomography in Gamma Knife Icon radiosurgery. *Phys. Medica* **52**, 93–97 (2018).

43. Nayak, L., Lee, E. Q. & Wen, P. Y. Epidemiology of brain metastases. *Curr. Oncol. Rep.* **14**, 48–54 (2012).

44. Chamberlain, M. C., Baik, C. S., Gadi, V. K., Bhatia, S. & Chow, L. Q. M. Systemic therapy of brain metastases: non–small cell lung cancer, breast cancer, and melanoma. *Neuro. Oncol.* **19**, i1–i24 (2016).

45. Patchell, R. A. *et al.* A Randomized Trial of Surgery in the Treatment of Single Metastases to the Brain. *N. Engl. J. Med.* **322**, 494–500 (1990).

46. Vecht, C. J. *et al.* Treatment of single brain metastasis: Radiotherapy alone or combined with neurosurgery. *Ann. Neurol.* **33**, 583–590 (1993).

47. Lassen, B. *et al.* Surgical mortality at 30 days and complications leading to recraniotomy in 2630 consecutive craniotomies for intracranial tumors. *Neurosurgery* **68**, 1259–1269 (2011).

48. Mintz, A., Perry, J., Spithoff, K., Chambers, A. & Laperriere, N. Management of single brain metastasis: a practice guideline. *Curr. Oncol.* **14**, 131 (2007).

49. Bhatnagar, A. K., Flickinger, J. C., Kondziolka, D. & Lunsford, L. D. Stereotactic radiosurgery for four or more intracranial metastases. *Int. J. Radiat. Oncol. Biol. Phys.* **64**, 898–903 (2006).

50. Minniti, G., Scaringi, C. & Maurizi Enrici, R. Radiation techniques for acromegaly. *Radiat Oncol* **6**, (2011).

51. Tsao, M., Xu, W. & Sahgal, A. A meta-analysis evaluating stereotactic radiosurgery, whole-brain radiotherapy, or both for patients presenting with a limited number of brain metastases. *Cancer* **118**, 2486–2493 (2012).

52. O'Neill, B. P. *et al.* A comparison of surgical resection and stereotactic radiosurgery in the treatment of solitary brain metastases. *Int. J. Radiat. Oncol. Biol. Phys.* **55**, 1169–1176 (2003).

53. Yamamoto, M. *et al.* Gamma knife radiosurgery with numerous target points for intracranially disseminated metastases. in *Radiosurgery 1997* **2**, 94–109 (Karger Publishers, 1998).

54. Thumma, S. R. *et al.* Long-term survival after gamma knife radiosurgery in a case of recurrent glioblastoma multiforme: a case report and review of the literature. *Case Rep. Med.* **2012**, (2012).

55. Redmond, K. J. & Mehta, M. Stereotactic Radiosurgery for Glioblastoma. *Cureus* **7**, e413–e413 (2015).

56. Crowley, R. W., Pouratian, N. & Sheehan, J. P. Gamma knife surgery for

glioblastoma multiforme. *Neurosurg. Focus FOC* **20**, E17 (2006).

57. Larson, D. A., Flickinger, J. C. & Loeffler, J. S. Radiobiology of radiosurgery. *Int J Radiat Oncol Biol Phys* **25**, (1993).

58. Su, C.-F., Liu, D.-W., Lee, C.-C. & Chiu, T.-L. Volume-staged gamma knife surgery for the treatment of large skull base meningioma surrounding the optical apparatus: a snowman-shape design. *J. Chinese Med. Assoc.* **80**, 697–704 (2017).

59. Mak, H. K.-F. *et al.* Effective time window in reducing pituitary adenoma size by gamma knife radiosurgery. *Pituitary* **18**, 509–517 (2015).

60. Mortini, P., Losa, M., Barzaghi, R., Boari, N. & Giovanelli, M. Results of transsphenoidal surgery in a large series of patients with pituitary adenoma. *Neurosurgery* **56**, 1222–1233 (2005).

61. Laws, E. R. *et al.* Stereotactic radiosurgery for pituitary adenomas: a review of the literature. *J. Neurooncol.* **69**, 257–272 (2004).

62. Losa, M. *et al.* Gamma knife surgery for treatment of residual nonfunctioning pituitary adenomas after surgical debulking. *J. Neurosurg.* **100**, 438–444 (2004).

63. Sheehan, J. P., Pouratian, N., Steiner, L., Laws, E. R. & Vance, M. L. Gamma Knife surgery for pituitary adenomas: factors related to radiological and endocrine outcomes. *J. Neurosurg.* **114**, 303–309 (2011).

64. Franzin, A., Spatola, G., Losa, M., Picozzi, P. & Mortini, P. Results of gamma knife radiosurgery in acromegaly. *Int. J. Endocrinol.* **2012**, (2012).

65. Pollock, B. E., Phuong, L. K., Gorman, D. A., Foote, R. L. & Stafford, S. L. Stereotactic radiosurgery for idiopathic trigeminal neuralgia. *J. Neurosurg.* **97**, 347–353 (2002).

66. Kim, M. *et al.* Gamma Knife surgery for invasive pituitary macroadenoma. *J. Neurosurg.* **105**, 26–30 (2006).

67. Sweeney, P., Yajnik, S., Hartsell, W., Bovis, G. & Venkatesan, J. Stereotactic radiotherapy for vestibular schwannoma. *Otolaryngol. Clin. North Am.* **42**, 655–663 (2009).

68. Williams, B. J. *et al.* Gamma Knife surgery for large vestibular schwannomas: a single-center retrospective case-matched comparison assessing the effect of lesion size. *J. Neurosurg.* **119**, 463–471 (2013).

69. Kondziolka, D., Lunsford, L. D., Mclaughlin, M. R. & Flickinger, J. C. Long-term outcomes after radiosurgery for acoustic neuromas. *N. Engl. J. Med.* **339**, 1426–1433 (1998).

70. Flickinger, J. C., Kondziolka, D., Niranjan, A. & Lunsford, L. D. Results of acoustic neuroma radiosurgery: an analysis of 5 years' experience using current methods. *J. Neurosurg.* **94**, 1–6 (2001).

71. Flickinger, J. C. *et al.* Acoustic neuroma radiosurgery with marginal tumor doses of 12 to 13 Gy. *Int. J. Radiat. Oncol. Biol. Phys.* **60**, 225–230 (2004).

72. Roos, D. E., Potter, A. E. & Brophy, B. P. Stereotactic radiosurgery for acoustic neuromas: What happens long term? *Int. J. Radiat. Oncol. Biol. Phys.* **82**, 1352–1355 (2012).

73. Chung, L. K. *et al.* Impact of Cochlear Dose on Hearing Preservation following Stereotactic Radiosurgery and Fractionated Stereotactic Radiotherapy for the Treatment of Vestibular Schwannoma. *J. Neurol. Surg. Part B Skull Base* **79**, 335–342 (2018).

74. Yomo, S., Tamura, M., Carron, R., Porcheron, D. & Régis, J. A quantitative comparison of radiosurgical treatment parameters in vestibular schwannomas: the Leksell Gamma Knife Perfexion versus Model 4C. *Acta Neurochir. (Wien).* **152**, 47–55 (2010).

75. Stieber, V. *et al.* Determination of a clinical value for the repair half-time (T1/2) of the trigeminal nerve based on outcome data from gamma knife radiosurgery for facial pain. *Radiat. Res.* **168**, 143–148 (2007).

76. Aubuchon, A. C. *et al.* Repeat gamma knife radiosurgery for trigeminal neuralgia. *Int. J. Radiat. Oncol. Biol. Phys.* **81**, 1059–1065 (2011).

77. Pokhrel, D. *et al.* Linac-based stereotactic radiosurgery (SRS) in the treatment of refractory trigeminal neuralgia: Detailed description of SRS procedure and reported clinical outcomes. *J. Appl. Clin. Med. Phys.* **18**, 136–143 (2017).

78. Hall, E. J. & Giaccia, A. J. *Radiobiology for the Radiologist.* **6**, (Lippincott Williams & Wilkins, 2006).

79. Lee, S. P. *et al.* Biologically effective dose distribution based on the linear quadratic model and its clinical relevance. *Int. J. Radiat. Oncol. Biol. Phys.* **33**, 375–389 (1995).

80. Joiner, M. C. & Van der Kogel, A. *Basic clinical radiobiology.* (CRC press, 2009).

81. Niranjan, A. & Flickinger, J. C. Radiobiology, principle and technique of radiosurgery. *Prog. Neurol. Surg.* **21**, 32–42 (2008).

82. Jiménez-Franco, L. D. Development of a treatment planning algorithm for peptide-receptor radionuclide therapy considering multiple tumour lesions and organs at risk. (Heidelberg University, 2018). doi:DOI: https://doi.org/10.11588/heidok.00025709

83. Brenner, D. J., Hlatky, L. R., Hahnfeldt, P. J., Huang, Y. & Sachs, R. K. The linear-quadratic model and most other common radiobiological models result in similar predictions of time-dose relationships. *Radiat. Res.* **150**, 83–91 (1998).

84. Barendsen, G. W. Dose fractionation, dose rate and iso-effect relationships for normal tissue responses. *Int. J. Radiat. Oncol. Biol. Phys.* **8**, 1981–1997 (1982).

85. Fowler, J. F. Fractionation and therapeutic gain. in *The biological basis of radiotherapy. Second edition* (1989).

86. Buckle, A. H. & Lewis, J. Biologically effective dose using reciprocal repair for varying fraction doses and fraction intervals. *Br. J. Radiol.* **81**, 137–142 (2008).

87. Deasy, J. O., Blanco, A. I. & Clark, V. H. CERR: A computational environment for radiotherapy research. *Med. Phys.* **30**, 979–985 (2003).

88. Aly, M. M. O. M., Abo-Madyan, Y., Jahnke, L., Wenz, F. & Glatting, G. Comparison of breast sequential and simultaneous integrated boost using the biologically effective dose volume histogram (BEDVH). *Radiat. Oncol.* **11**, 16 (2016).

89. Bender, E. T. Brain necrosis after fractionated radiation therapy: Is the halftime for repair longer than we thought. *Med. Phys.* **39**, 7055–7061 (2012).

90. Nokhasteh, S., Nazemi, H., Hejazi, P. & Dayyani, M. Comparison of Dosimetric Parameters Between Field in Field and Conformal Radiation Therapy Techniques in Early Stage of Left Breast Cancer Patients. *Int. J. Cancer Manag.* **12**, (2019).

91. Jiménez-Franco, L. D., Kletting, P., Beer, A. J. & Glatting, G. Treatment planning algorithm for peptide receptor radionuclide therapy considering multiple tumor lesions and organs at risk. *Med. Phys.* **45**, 3516–3523 (2018).

92. Qi, X. S., Schultz, C. J. & Li, X. A. An estimation of radiobiologic parameters from clinical outcomes for radiation treatment planning of brain tumor. *Int. J. Radiat. Oncol.* **64**, 1570–1580 (2006).

93. Fowler, J. F. Repair between dose fractions: A simpler method of analyzing and reporting apparently biexponential repair. *Radiat. Res.* **158**, 141–151 (2002).

94. Prabhakar, R. & Rath, G. K. A simple plan evaluation index based on the dose to critical structures in radiotherapy. *J. Med. Physics/Association Med. Phys.*

India **36**, 192 (2011).

95.   Emami, B. *et al.* Tolerance of normal tissue to therapeutic irradiation. *Int. J. Radiat. Oncol. Biol. Phys.* **21**, 109–122 (1991).

96.   Tishler, R. B. *et al.* Tolerance of cranial nerves of the cavernous sinus to radiosurgery. *Int. J. Radiat. Oncol. Biol. Phys.* **27**, 215–221 (1993).

97.   De Marzi, L. *et al.* Use of gEUD for predicting ear and pituitary gland damage following proton and photon radiation therapy. *Br. J. Radiol.* **88**, 20140413 (2015).

98.   Lee, J. Y. K. *et al.* Higher dose rate Gamma Knife radiosurgery may provide earlier and longer-lasting pain relief for patients with trigeminal neuralgia. *J. Neurosurg.* **123**, 961–968 (2015).

99.   Smith, D. R. *et al.* Treatment outcomes and dose rate effects following gamma knife stereotactic radiosurgery for vestibular schwannomas. *Neurosurgery* **85**, E1084–E1094 (2019).

100. Hopewell, J. W., Millar, W. T. & Lindquist, C. Radiobiological principles: their application to gamma knife therapy. in *Current and Future Management of Brain Metastasis* **25**, 39–54 (Karger Publishers, 2012).

101. Putora, P. M., Schmuecking, M., Aebersold, D. & Plasswilm, L. Compensability index for compensation radiotherapy after treatment interruptions. *Radiat. Oncol.* **7**, 208 (2012).

8 APPENDIX

8.1 Therapeutic effect of using the optimal shot sequence and a mono-exponential repair model

8.1.1 Patients with defined OARs

Table 8 The therapeutic index values for the clinical sequences and optimal sequences for the nine patients with defined OARs. The optimal shot sequence was defined as the sequence leading to the highest therapeutic index. The oBED values used to calculate the therapeutic indices were calculated using the mono-exponential repair model.

Patient	Therapeutic index		% change
	Clinical	Optimal	
1 [a]	7.96	8.06	+1.3
2 [e]	7.62	8.04	+5.5
3 [a]	2.19	2.26	+3.2
4 [a]	2.27	2.32	+2.2
5 [f]	0.52	0.55	+5.8
6 [g]	40.09	44.10	+10
7 [c]	10.03	10.05	+0.2
8 [h]	34.67	37.34	+7.7
9 [c]	13.79	14.05	+1.9

[a] Cochlea   [c] Brainstem   [e] Trigeminal Nerve
[f] Cochlea Nerve   [g] Medulla   [h] Pituitary gland

Table 9 The oBED values for the clinical sequences and the optimal sequences for the nine patients with defined OARs. The optimal shot sequence was defined as the sequence leading to the highest therapeutic index. The oBED values for the target and the dose-limiting OAR were calculated using the mono-exponential repair model.

Patient	Target oBED (Gy_{10})		OAR oBED ($Gy_{2.47}$)	
	Clinical	Optimal	Clinical	Optimal
1 [a]	33.33	39.91	4.19	4.20
2 [e]	26.64	28.88	3.50	3.60
3 [a]	28.34	29.47	12.92	13.04
4 [a]	35.38	35.94	15.62	15.51
5 [f]	29.98	31.63	57.72	57.72
6 [g]	44.52	47.38	1.11	1.07
7 [c]	14.00	13.97	1.40	1.39
8 [h]	62.35	64.32	1.80	1.72
9 [c]	48.55	49.68	3.52	3.54

[a] Cochlea   [c] Brainstem   [e] Trigeminal Nerve
[f] Cochlear Nerve   [g] Medulla   [h] Pituitary gland

8.1.2 Patients with no defined OAR

Table 10 Target oBED values for the clinical sequences and the optimal sequences for the 16 patients with no OAR defined. The optimal shot sequence was defined as the sequence leading to the highest target oBED. The target oBED values were calculated using the mono-exponential repair model.

Patient	Target oBED (Gy_{10})		% change
	Clinical	Optimal	
10	49.83	50.98	+2.3
11	44.89	47.04	+4.8
12	42.72	47.91	+12.1
13	64.27	65.80	+2.4
14	69.18	73.13	+5.7
15	51.65	54.41	+5.3
16	79.28	82.52	+4.1
17	57.99	61.58	+6.2
18	64.38	66.06	+2.6
19	65.5	67.99	+3.8
20	75.83	78.04	+2.9
21	25.93	26.49	+2.2
22	16.09	16.48	+2.4
23	25.27	26.86	+6.3
24	24.85	25.97	+4.5
25	63.48	64.48	+1.6

8.2 Therapeutic effect of using the optimal shot sequence and a reciprocal repair model

8.2.1 Patients with defined OARs

Table 11 The therapeutic index values for the clinical sequences and optimal sequences for the nine patients with defined OARs. The optimal shot sequence was defined as the sequence leading to the highest therapeutic index. The oBED values used to calculate the therapeutic indices were calculated using the reciprocal repair model.

Patient	Therapeutic index		% change
	Clinical	Optimal	
1 [a]	7.92	8.01	+1.1
2 [e]	7.71	8.06	+4.5
3 [a]	2.19	2.24	+2.3
4 [a]	2.27	2.30	+1.3
5 [f]	0.51	0.53	+3.9
6 [g]	42.95	44.58	+3.8
7 [c]	8.39	8.42	+0.4
8 [h]	35.62	37.38	+4.9
9 [c]	13.85	14.06	+1.5

[a] Cochlea   [c] Brainstem   [e] Trigeminal Nerve
[f] Cochlear Nerve   [g] Medulla   [h] Pituitary gland

Table 12 The oBED values for the clinical sequences and the optimal sequences for the nine patients with defined OARs. The optimal shot sequence was defined as the sequence leading to the highest therapeutic index. The oBED values for the target and the dose-limiting OAR were calculated using the reciprocal repair model.

Patient	Target oBED (Gy_{10})		OAR oBED ($Gy_{2.47}$)	
	Clinical	Optimal	Clinical	Optimal
1 [a]	34.15	34.60	4.31	4.33
2 [e]	28.11	29.80	3.64	3.70
3 [a]	29.11	29.97	13.30	13.37
4 [a]	36.01	36.44	15.89	15.83
5 [f]	31.44	32.62	62.07	62.07
6 [g]	47.78	49.75	1.11	1.12
7 [c]	14.03	14.10	1.67	1.68
8 [h]	67.53	69.20	1.90	1.85
9 [c]	49.07	49.92	3.54	3.55

[a] Cochlea [c] Brainstem [e] Trigeminal Nerve
[f] Cochlear Nerve [g] Medulla [h] Pituitary gland

8.2.2 Patients with no defined OAR

Table 13 Target oBED values for the clinical sequences and the optimal sequences for the 16 patients with no OAR defined. The optimal shot sequence was defined as the sequence leading to the highest target oBED. The target oBED values were calculated using the reciprocal repair model.

Patient	Target oBED (Gy_{10})		% change
	Clinical	Optimal	
10	51.48	52.33	+1.7
11	47.08	48.55	+3.1
12	46.10	49.96	+8.4
13	66.79	67.83	+1.6
14	71.91	74.79	+4.0
15	52.62	54.76	+4.1
16	81.12	83.66	+3.1
17	61.13	63.59	+4.0
18	65.93	67.12	+1.8
19	66.81	68.60	+2.7
20	77.90	79.51	+2.1
21	26.84	27.13	+1.1
22	16.68	16.96	+1.7
23	26.65	27.79	+4.3
24	26.46	27.19	+2.8
25	66.55	67.19	+1.0

8.3 Therapeutic effect of using the optimal shot sequence and a bi-exponential repair model

8.3.1 Patients with defined OARs

Table 14 Therapeutic index values for the clinical and the optimal sequences for the nine patients with defined OARs. The optimal shot sequence was defined as the sequence leading to the highest therapeutic index. The oBED values used to calculate the therapeutic indices were calculated using the bi-exponential repair model.

| Patient | Therapeutic index | | % change |
	Clinical	Optimal	
1 [a]	8.65	8.71	+0.7
2 [e]	9.75	9.95	+2.1
3 [a]	2.55	2.66	+4.3
4 [a]	2.74	2.95	+7.7
5 [f]	0.74	0.78	+5.4
6 [g]	38.41	41.06	+6.9
7 [c]	8.53	8.62	+1.1
8 [h]	26.35	27.16	+3.1
9 [c]	11.59	11.68	+0.8

[a] Cochlea   [c] Brainstem [e] Trigeminal Nerve
[f] Cochlear Nerve   [g] Medulla   [h] Pituitary gland

Table 15 The oBED values for the clinical sequences and the optimal sequences for the nine patients with defined OARs. The optimal shot sequence was defined as the sequence leading to the highest therapeutic index. The oBED values for the target and the dose-limiting OAR were calculated using the bi-exponential repair model.

| Patient | Target oBED ($Gy_{8.31}$) | | OAR oBED ($Gy_{2.47}$) | |
	Clinical	Optimal	Clinical	Optimal
1 [a]	28.52	28.70	3.30	3.29
2 [e]	27.10	26.74	2.78	2.69
3 [a]	25.67	25.96	10.07	9.76
4 [a]	35.70	35.29	13.01	11.97
5 [f]	25.01	25.42	33.6	32.77
6 [g]	38.16	38.78	0.99	0.94
7 [c]	13.51	13.47	1.58	1.56
8 [h]	40.81	41.85	1.55	1.54
9 [c]	38.58	37.82	3.33	3.22

[a] Cochlea   [c] Brainstem   [e] Trigeminal Nerve
[f] Cochlear Nerve   [g] Medulla   [h] Pituitary gland

8.3.2 Patients with no defined OAR

Table 16 Target oBED values for the clinical sequences and the optimal sequences for the 16 patients with no OAR defined. The optimal shot sequence was defined as the sequence leading to the highest target oBED. The target oBED values were calculated using the bi-exponential repair model.

Patient	Target oBED ($Gy_{8.31}$)		% change
	Clinical	Optimal	
10	37.38	37.91	+1.4
11	30.87	31.87	+3.2
12	40.87	45.35	+11.0
13	51.52	52.62	+2.1
14	53.74	55.99	+4.2
15	40.08	41.32	+3.1
16	69.18	71.62	+3.5
17	38.70	40.17	+3.8
18	41.06	41.76	+1.7
19	41.30	42.31	+2.4
20	58.95	59.57	+1.1
21	22.41	22.99	+2.6
22	14.61	14.70	+0.6
23	22.59	23.23	+2.8
24	16.12	16.36	+1.5
25	49.82	50.39	+1.1

8.4 Therapeutic effect of using decayed Gamma Knife sources and a mono-exponential repair model

8.4.1 Patients with defined OARs

Table 17 The therapeutic index values for the clinical sequences and optimal sequences for the nine patients with defined OARs. The optimal shot sequence was defined as the sequence leading to the highest therapeutic index. The oBED values used to calculate the therapeutic indices were calculated using the mono-exponential repair model and considering source decay after one half-life from the original activity.

Patient	Therapeutic index		% change
	Clinical	Optimal	
1 [a]	7.58	7.73	+2.0
2 [e]	7.24	7.67	+5.9
3 [a]	2.08	2.17	+4.3
4 [a]	2.15	2.23	+3.7
5 [f]	0.52	0.56	+7.7
6 [g]	36.90	41.24	+11.8
7 [c]	8.26	8.31	+0.6
8 [h]	35.05	36.82	+5.0
9 [c]	13.28	13.61	+2.5

[a] Cochlea   [c] Brainstem   [e] Trigeminal Nerve
[f] Cochlear Nerve   [g] Medulla   [h] Pituitary gland

Table 18 The oBED values for the clinical sequences and the optimal sequences for the nine patients with defined OARs. The optimal shot sequence was defined as the sequence leading to the highest therapeutic index. The oBED values for the target and the dose-limiting OAR were calculated using the mono-exponential repair model and considering source decay after one half-life from the original activity.

	Target oBED (Gy_{10})		OAR oBED ($Gy_{2.47}$)	
Patient	Clinical	Optimal	Clinical	Optimal
1 [a]	30.13	30.71	3.97	3.97
2 [e]	23.72	26.37	3.28	3.44
3 [a]	25.48	26.41	12.24	12.18
4 [a]	32.43	33.24	15.11	14.91
5 [f]	26.68	28.21	50.95	50.22
6 [g]	39.70	41.78	1.08	1.01
7 [c]	13.64	13.76	1.65	1.66
8 [h]	59.23	59.59	1.69	1.62
9 [c]	46.19	47.74	3.48	3.51

[a] Cochlea   [c] Brainstem   [e] Trigeminal Nerve
[f] Cochlear Nerve   [g] Medulla   [h] Pituitary gland

8.4.2 Patients with no defined OAR

Table 19 Target oBED values for the clinical sequences and the optimal sequences for the 16 patients with no OAR defined. The optimal shot sequence was defined as the sequence leading to the highest target oBED. The target oBED values were calculated using the mono-exponential repair model and considering the effect of source decay after one half-life from the original activity.

	Target oBED (Gy_{10})		
Patient	Clinical	Optimal	% change
10	44.67	46.12	+3.2
11	39.74	42.08	+5.9
12	39.38	43.34	+10.1
13	57.38	58.71	+2.3
14	61.68	66.27	+7.4
15	47.44	51.54	+8.6
16	71.15	75.63	+6.3
17	53.59	56.54	+5.5
18	58.98	61.12	+3.6
19	61.23	64.43	+5.2
20	68.10	71.11	+4.4
21	23.27	23.86	+2.5
22	14.63	15.10	+3.2
23	22.71	24.34	+7.2
24	22.44	23.57	+5.0
25	55.51	56.50	+1.8

8.5 Therapeutic effect of using decayed Gamma Knife sources and a reciprocal repair model Patients with defined OARs

8.5.1 Patients with defined OARs

Table 20 The therapeutic index values for the clinical sequences and optimal sequences for the nine patients with defined OARs. The optimal shot sequence was defined as the sequence leading to the highest therapeutic index. The oBED values used to calculate the therapeutic indices were calculated using the reciprocal repair model and considering source decay after one half-life from the original activity.

Patient	Therapeutic index		% change
	Clinical	Optimal	
1 [a]	7.59	7.70	+1.4
2 [e]	7.37	7.72	+4.7
3 [a]	2.09	2.15	+2.9
4 [a]	2.17	2.22	+2.3
5 [f]	0.50	0.52	+4.0
6 [g]	39.57	42.46	+7.3
7 [c]	8.25	8.29	+0.5
8 [h]	35.13	36.88	+5.0
9 [c]	13.45	13.69	+1.8

[a] Cochlea   [c] Brainstem   [e] Trigeminal Nerve
[f] Cochlear Nerve   [g] Medulla   [h] Pituitary gland

Table 21 The oBED values for the clinical sequences and the optimal sequences for the nine patients with defined OARs. The optimal shot sequence was defined as the sequence leading to the highest therapeutic index. The oBED values for the target and the dose-limiting OAR were calculated using the reciprocal repair model and considering source decay after one half-life from the original activity.

Patient	Target oBED (Gy_{10})		OAR oBED ($Gy_{2.47}$)	
	Clinical	Optimal	Clinical	Optimal
1 [a]	31.87	32.45	4.20	4.21
2 [e]	25.96	27.92	3.52	3.62
3 [a]	27.06	28.12	12.95	13.06
4 [a]	33.86	34.44	15.62	15.51
5 [f]	29.10	30.45	58.40	58.43
6 [g]	44.16	46.18	1.12	1.09
7 [c]	13.74	13.83	1.67	1.67
8 [h]	64.24	65.45	1.83	1.77
9 [c]	47.36	48.42	3.52	3.54

[a] Cochlea   [c] Brainstem   [e] Trigeminal Nerve
[f] Cochlear Nerve   [g] Medulla   [h] Pituitary gland

8.5.2 Patients with no defined OAR

Table 22 Target oBED values for the clinical sequences and the optimal sequences for the 16 patients with no OAR defined. The optimal shot sequence was defined as the sequence leading to the highest target oBED. The target oBED values are calculated using the reciprocal repair model and considering the effect of source decay after one half-life from the original activity.

| Patient | Target oBED (Gy_{10}) | | % change |
	Clinical	Optimal	
10	47.90	48.91	+2.1
11	43.54	45.17	+3.7
12	42.99	46.60	+8.4
13	61.88	62.86	+1.6
14	66.77	70.06	+4.9
15	49.66	52.56	+5.8
16	75.26	78.53	+4.3
17	58.01	60.37	+4.1
18	62.28	63.68	+2.2
19	63.93	66.05	+3.3
20	72.54	74.57	+2.8
21	24.90	25.33	+1.7
22	15.62	15.95	+2.1
23	24.74	25.96	+4.9
24	24.64	25.44	+3.2
25	60.92	61.59	+1.1

8.6 Therapeutic effect of using decayed Gamma Knife sources and a bi-exponential repair model

8.6.1 Patients with defined OARs

Table 23 The therapeutic index values for the clinical sequences and optimal sequences for the nine patients with defined OARs. The optimal shot sequence was defined as the sequence leading to the highest therapeutic index. The oBED values used to calculate the therapeutic indices were calculated using the bi-exponential repair model and considering source decay after one half-life from the original activity.

| Patient | Therapeutic index | | % change |
	Clinical	Optimal	
1 [a]	9.15	9.22	+0.8
2 [e]	9.62	9.75	+1.4
3 [a]	2.72	2.80	+2.9
4 [a]	2.94	3.11	+5.8
5 [f]	0.86	0.89	+3.5
6 [g]	38.40	40.35	+5.1
7 [c]	8.73	8.85	+1.4
8 [h]	25.53	26.53	+3.9
9 [c]	11.65	11.66	+0.1

[a] Cochlea   [c] Brainstem   [e] Trigeminal Nerve
[f] Cochlear Nerve   [g] Medulla   [h] Pituitary gland

Table 24 The oBED values for the clinical sequences and the optimal sequences for the nine patients with defined OARs. The optimal shot sequence was defined as the sequence leading to the highest therapeutic index. The oBED values for the target and the dose-limiting OAR are calculated using the bi-exponential repair model and considering the effect of source decay after one half-life from the original activity.

Patient	Target oBED ($Gy_{8.31}$)		OAR oBED ($Gy_{2.47}$)	
	Clinical	Optimal	Clinical	Optimal
1 [a]	27.36	27.61	2.99	2.99
2 [e]	25.40	25.59	2.64	2.62
3 [a]	24.57	25.03	9.04	8.93
4 [a]	33.97	33.45	11.57	10.76
5 [f]	23.72	24.13	27.65	27.13
6 [g]	36.75	37.70	0.96	0.93
7 [c]	13.29	13.24	1.52	1.50
8 [h]	39.10	40.73	1.53	1.54
9 [c]	37.79	38.20	3.24	3.28

[a] Cochlea   [c] Brainstem   [e] Trigeminal Nerve
[f] Cochlear Nerve   [g] Medulla   [h] Pituitary gland

8.6.2 Patients with no defined OAR

Table 25 Target oBED values for the clinical sequences and the optimal sequences for the 16 patients with no OAR defined. The optimal shot sequence was defined as the sequence leading to the highest target oBED. The target oBED values were calculated using the bi-exponential repair model and considering the effect of source decay after one half-life from the original activity.

Patient	Target oBED ($Gy_{8.31}$)		% change
	Clinical	Optimal	
10	35.72	36.38	+1.8
11	28.81	29.54	+2.5
12	36.92	40.27	+9.1
13	47.98	49.38	+2.9
14	51.08	53.98	+5.7
15	38.56	40.20	+4.3
16	65.65	68.79	+4.8
17	37.10	38.94	+5.0
18	39.52	40.41	+2.3
19	40.14	41.43	+3.2
20	56.47	57.29	+1.5
21	21.56	22.09	+2.5
22	13.96	14.09	+0.9
23	21.28	22.11	+3.9
24	15.39	15.69	+1.9
25	46.53	47.21	+1.5

8.7 Optimal shot sequences

Table 26 Optimal shot sequences leading to the highest therapeutic index or to the highest target oBED. oBED values were calculated with three sublethal repair models: mono-exponential, reciprocal and bi-exponential. oBED values were used for the target and for the calculation of the therapeutic indices.

Patient	Mono-exponential		Reciprocal	Bi-exponential
	Clinical	Optimal	Optimal	Optimal
1*	1-2-3-4-5-6	3-1-5-2-4-6	3-1-5-2-4-6	1-5-3-2-4-6
2*	1-2-3-4-5-6	2-5-1-4-3-6	5-2-1-4-3-6	6-4-5-2-3-1
3*	1-2-3-4-5-6-7	3-7-5-2-4-6-1	3-7-5-2-4-6-1	1-6-3-7-5-2-4
4*	1-2-3-4	2-1-4-3	2-1-4-3	3-1-2-4
5*	1-2-3-4-5-6-7	7-4-5-2-1-6-3	7-4-5-2-1-6-3	2-7-3-4-5-1-6
6*	1-2-3-4-5-6-7	5-6-1-4-3-2-7	5-6-1-4-3-2-7	5-1-4-3-6-2-7
7*	1-2-3-4-5-6	2-1-5-3-4-6	6-4-3-1-2-5	2-3-1-6-4-5
8*	1-2-3-4-5-6	2-5-1-4-3	2-5-1-4-3	2-4-1-3-5
9*	1-2-3-4	4-3-1-2	4-3-1-2	2-4-3-1
10$	1-2-3-4-5	2-5-4-3-1	2-5-4-3-1	2-4-5-3-1
11$	1-2-3-4-5-6	6-4-2-1-3-5	6-4-2-1-3-5	3-6-5-4-2-1
12$	1-2-3-4-5-6-7	7-6-3-2-4-5-1	7-6-3-2-4-5-1	3-2-6-7-5-4-1
13$	1-2-3-4-5-6	3-4-2-5-1-6	3-4-2-5-1-6	4-1-5-2-6-3
14$	1-2-3-4-5	5-4-1-2-3	5-4-1-2-3	5-2-4-1-3
15$	1-2-3-4-5-6	6-5-4-3-2-1	6-5-4-3-2-1	5-6-4-2-3-1
16$	1-2-3-4-5	5-2-4-1-3	5-2-4-1-3	5-4-1-3-2
17$	1-2-3-4	2-4-1-3	2-4-1-3	2-4-1-3
18$	1-2-3-4-5	5-3-2-4-1	5-3-2-4-1	5-1-4-2-3
19$	1-2-3-4	3-4-1-2	3-4-1-2	3-1-4-2
20$	1-2-3-4-5	5-1-3-2-4	5-1-3-2-4	5-1-3-2-4
21$	1-2-3-4-5-6-7-8-9-10-11-12-13-14-15-16-17	15-10-2-8-7-9-1-11-1-12- 5-4-3-6-16-14-17	15-10-2-8-7-9-1-11-1-12- 5-4-3-6-16-14-17	15-10-2-8-7-9-1-11-1-12- 5-4-3-6-16-14-17
22$	1-2-3-4-5-6-7-8-9-10-11-12-13-14-15-16-17-18-19-20	9-8-17-11-4-19-2-13-7-10-16-6-1-5-12-15-14-20-18-3	9-8-17-11-4-19-2-13-7-10-16-6-1-5-12-15-14-20-18-3	12-17-15-6-19-20-5-18-13-3-1-11-4-10-9-2-16-14-8-7
23$	1-2-3-4-5-6-7-8-9-10-11-12-13-14-15-16-17-18-19-20-21-22-23-24-25	7-19-9-16-25-14-2-24-18-10-13-22-5-11-8-23-12-1-3-15-20-4-6-21-17	7-19-9-16-25-14-2-24-18-10-13-22-5-11-8-23-12-1-3-15-20-4-6-21-17	18-8-20-3-6-19-5-21-12-1-14-25-2-9-23-16-4-10-24-7-13-22-11-17-15
24$	1-2-3-4-5-6-7-8-9-10-11-12-13-14-15-16-17-18-19-20-21-22-23-24-25-26-27	10-2-26-22-25-20-23-15-17-12-1-13-3-11-16-6-8-18-24-27-9-4-7-5-21-14-19	10-2-26-22-25-20-23-15-17-12-1-13-3-11-16-6-8-18-24-27-9-4-7-5-21-14-19	10-2-26-22-25-20-23-15-17-12-1-13-3-11-16-6-8-18-24-27-9-4-7-5-21-14-19
25$	1-2-3-4-5-6-7-8-9-10-11-12-13-14-15-16-17-18-19-20-21-22-23-24-25-26-27-28-29-30-31-32-33	3-11-24-4-1-19-12-22-23-13-17-2-15-7-27-6-10-5-9-31-29-21-25-16-14-18-32-33-28-26-20-8-30	3-11-24-4-1-19-12-22-23-13-17-2-15-7-27-6-10-5-9-31-29-21-25-16-14-18-32-33-28-26-20-8-30	29-9-23-22-24-6-7-14-11-8-1-17-28-20-16-19-4-27-12-3-25-2-10-15-5-18-21-13-30-33-31-26-32

* Optimal sequence defined by the highest therapeutic index
$ Optimal sequence defined by the highest therapeutic target oBED

9   CURRICULUM VITAE

PERSONAL INFORMATION

First Name and Family Name:	Juliana Binti Mohd Radzi
Date of birth:	21 Feb 1985
Place of birth:	Kelantan, Malaysia

EDUCATION

2016- Present	PhD student in Medical Physics Medical Faculty Mannheim Heidelberg University, Heidelberg - Germany
2008-2009	Master of Science in Medical Physics Universiti Sains Malaysia (USM) – Penang, Malaysia CGPA: 3.55/4.0
2004-2008	Bachelor of Science (Hons) in Medical Radiation Universiti Sains Malaysia (USM) – Kelantan, Malaysia CGPA: 3.52/4.0
2003-2004	Certificate Science of Physics Matriculation college-Pahang, Malaysia CGPA:3.53/4.0

PROFESSIONAL EXPERIENCE

Dec/2009-Present	Undergraduate Lecturer School of Medical Imaging Faculty of Health Sciences Universiti Sultan Zainal Abidin (UniSZA), Terengganu, Malaysia
Sep-Dec/2009	Medical Physicist Department of Radiotherapy and Oncology Hospital Canselor Tuanku Muhriz UKM, Cheras, Kuala Lumpur, Malaysia

PUBLICATIONS

1. Hamizah NMZ, Juliana MR, Waidi AI, Ismalina SNI, Ahmad Z. Surface contamination in skin and room during hospitalization of thyroid cancer patient receiving radioiodine ablation. IOSR Journal of Dental and Medical Sciences (JDMS), Volume 2, Issue 1(Sept-Oct2012), PP27.33.

2. **J. Mohd Radzi**, G. Glatting, Z. Nasir, L.D. Jiménez-Franco, F.A. Giordano, F. Stieler. The effect of shot sequence on the biological effectiveness in Gamma Knife radiosurgery. DeGBS 2019. (Poster Presentation).

10 ACKNOWLEDGEMENT

First and most importantly, I want to thank God for giving me the opportunity to pursue and finish my studies, even though it seemed impossible at the beginning.

I would like to express my gratitude to Dr. Florian Stieler, Prof. Dr. Gerhard Glatting, Prof. Dr. Frederik Wenz and Dr. Luis David Jiménez, who played a significant role in supervising this thesis. Their advanced knowledge in critical writing, thesis construction and data analysis made this thesis become possible. Without their help and guidance, I would have not been able to finish it until the end.

I would like to thank my fellow friends Zulfa Nasir, Buthayna Alnaalwa, Dr. Bedor Abualhaj and Dr. Ali Asgar Attarwala for the fruitful discussions and for sharing ideas. It was great to support each other through the ups and down of this challenging journey.

Finally, special acknowledgements also go to my beloved parents, my husband (Mohd Jaffri Bin Abu Bakar), and my daughter (Inara Sofia) for believing in me and for their unconditional support. I am sorry for my daughter that I had to leave her and that I was apart from her throughout my study. For my late father, this is a gift to you even though you are no longer here, as I know that finishing my studies is also your wish for me. To all who have been mentioned and to those who have not been mentioned personally, these words are a symbol of my heartfelt gratitude.